ASTROBIOLOGY
Volume 22, Number 8, 2022

DOI: 10.1089/ast.2021.0078

The Bioburden and Ionic Composition of Hypersaline Lake Ices: Novel Habitats on Earth and Their Astrobiological Implications

Jacob J. Buffo,[1] Emma K. Brown,[2] Alexandra Pontefract,[3] Britney E. Schmidt,[4] Benjamin Klempay,[5] Justin Lawrence,[6] Jeff Bowman,[5] Meg Grantham,[6] Jennifer B. Glass,[6] Taylor Plattner,[6] Chase Chivers,[6] Peter Doran[7]; and the OAST Team

Abstract

We present thermophysical, biological, and chemical observations of ice and brine samples from five compositionally diverse hypersaline lakes in British Columbia's interior plateau. Possessing a spectrum of magnesium, sodium, sulfate, carbonate, and chloride salts, these low-temperature high-salinity lakes are analogs for planetary ice-brine environments, including the ice shells of Europa and Enceladus and ice-brine systems on Mars. As such, understanding the thermodynamics and biogeochemistry of these systems can provide insights into the evolution, habitability, and detectability of high-priority astrobiology targets. We show that biomass is typically concentrated in a layer near the base of the ice cover, but that chemical and biological impurities are present throughout the ice. Coupling bioburden, ionic concentration, and seasonal temperature measurements, we demonstrate that impurity entrainment in the ice is directly correlated to ice formation rate and parent fluid composition. We highlight unique phenomena, including brine supercooling, salt hydrate precipitation, and internal brine layers in the ice cover, important processes to be considered for planetary ice-brine environments. These systems can be leveraged to constrain the distribution, longevity, and habitability of low-temperature solar system brines—relevant to interpreting spacecraft data and planning future missions in the lens of both planetary exploration and planetary protection. Key Words: Brines—Ices—Planetary Analogs—Ice-Ocean Worlds—Mars—Halophilic Psychrophiles. Astrobiology 22, 962–980.

1. Introduction

1.1. Field site overview

The Interior Plateau of central British Columbia houses a diverse array of endorheic (closed basin) hypersaline lakes. Seasonal snowmelt and groundwater flow leaches metals and minerals from the local geology before collecting in the low-lying perennial and ephemeral lakes and playas, where the leachate concentrates and forms salts. The hot and arid summer climate of the region leads to substantial evaporation, and with minimal rainfall to refresh the lakes their salinities dramatically increase, reaching concentrations of 30–40% salt by weight.

In some cases, the lakes reach their saturation point and pure hydrated salts (*e.g.,* epsomite, mirabilite, meridianiite, natron, trona) begin to precipitate in the lake waters and underlying sediments (Renaut and Long, 1989). This cyclic concentrative process can lead to the formation of thick

[1]Thayer School of Engineering, Dartmouth College, Hanover, NH, USA.
[2]School of Earth and Space Exploration, Arizona State University, Pheonix, AZ, USA.
[3]Applied Physics Laboratory, John Hopkins University, Laurel, MD, USA.
[4]Department of Astronomy, Cornell University, Ithaca, NY, USA.
[5]Scripps Institution of Oceanography, La Jolla, CA, USA.
[6]School of Earth and Atmospheric Sciences, Georgia Institute of Technology, Atlanta, GA, USA.
[7]Department of Geology and Geophysics, Louisiung State University, Baton Rouge, LA, USA.

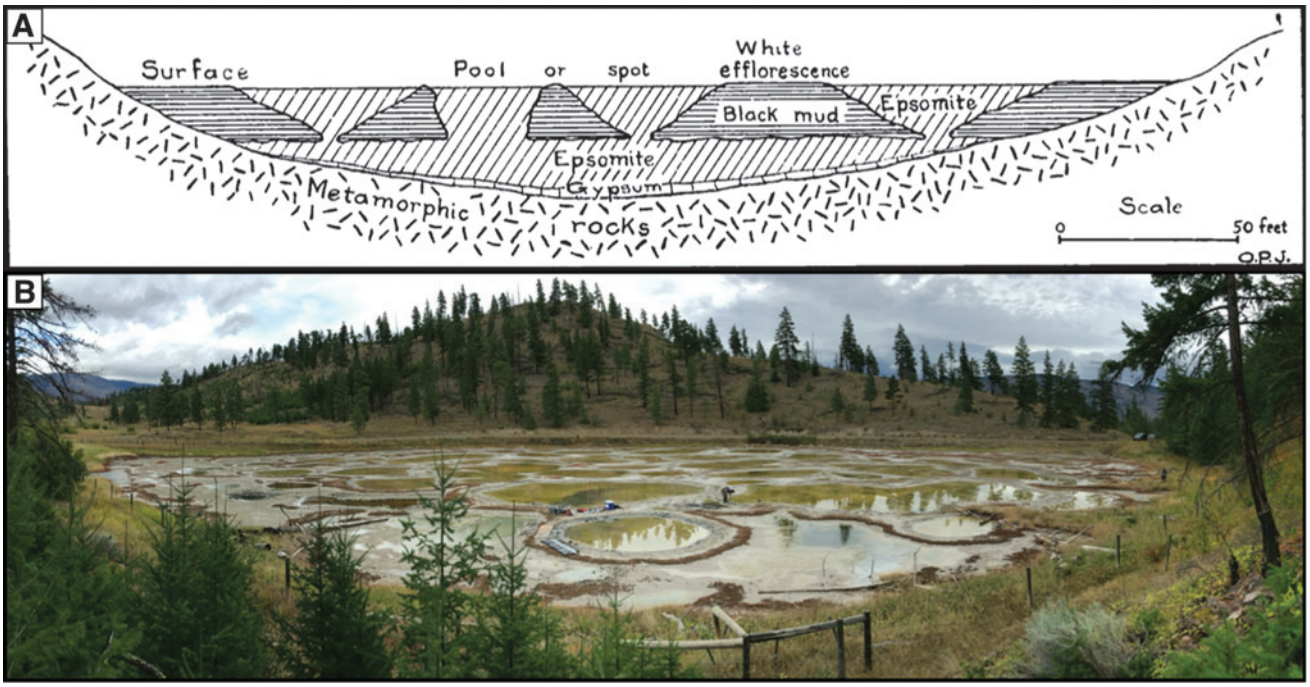

FIG. 1. Structure of the hypersaline lakes. **(A)** The subsurface structure of the spotted lakes, depicting the epsomite basement and columns/inverted cones that underlie the surficial pools, modified from Jenkins (1918). **(B)** Photograph of Basque Lake 2, taken in September 2019.

(~5 m), solid salt basements and columns beneath the lakes (Fig. 1) (Jenkins, 1918; Renaut and Long, 1989). Many lakes in this region exhibit a unique ''spotted'' morphology, where tens to hundreds of individual brine pools subdivide the lake (Fig. 1).

The formation process of the individual brine pools is currently unknown. Proposed formation mechanisms include density-driven subsidence caused by annual salt precipitation (Renaut and Long, 1989), bottom-up dendritic growth of sub-pool salt structures from the salt basement (Jenkins, 1918), and freeze-thaw processes in the shallow subsurface (Renaut and Long, 1989) akin to frost heave-driven patterned ground formation (Peterson and Krantz, 2008). Regardless of their origin, the brine pools are stable structures whose perimeters do not vary seasonally and have likely remained relatively unchanged over much longer timescales (~10–100 s of years) (Renaut and Long, 1989)

Although these extremely high salinity environments are toxic to many organisms, there exists a rich and unique halophilic ecosystem within each of the lakes (Pontefract *et al.*, 2017, 2019). As autumn ends, the resident organisms are subjected to an additional environmental stressor—extreme cold. With mean January temperatures ranging from –9°C to –12°C and nighttime lows that can exceed –45°C, the lakes form a substantial ice cover (Renaut and Long, 1989; Brown *et al.*, 2020a). The ice that forms from the hypersaline brines of these lakes is highly porous and contains both salts and organisms entrained during ice formation.

This process further concentrates the underlying brine, depressing its freezing point by as much as ~9°C, depending on the composition of the lake (Buffo *et al.*, 2019). The interstitial brine of the ice (brine contained in unfrozen pockets, channels, and grain boundaries) and the underlying brine reservoir constitute novel extreme environments that support a community of halophilic psychrophiles (Pontefract *et al.*, 2017, 2019; Buffo *et al.*, 2019).

The wintertime abundance and productivity of microfauna in this porous system is likely limited by physicochemical properties of the ice and brine, such as pore connectivity, water activity (A_w; a measure of the thermodynamic availability of water for microbial processes), and chaotropicity/kosmotropicity (a measure of the extent to which solutes disrupt or stabilize biological structures, respectively) (Weeks and Ackley, 1986; Loose *et al.*, 2011; Murray *et al.*, 2012; Stevens and Cockell, 2020).

The osmotic stress and potentially destabilizing (chaotropic) properties of hypersaline environments are well documented in the literature (Hallsworth *et al.*, 2007; Oren, 2013; Fisher *et al.*, 2021) and have even been discussed in the context of martian environments (Tosca *et al.*, 2008; Fox-Powell *et al.*, 2016; Pontefract *et al.*, 2017). These works emphasize the importance of the concentration and chemical composition of a brine in governing its habitability, as both A_w and chao-/kosmotropicity (strongly limiting factors for life as we know it [Pontefract *et al.*, 2017; Fox-Powell and Cockell, 2018]) are heavily dependent on the ionic species present. In complex multi-component brines, such as these lakes, the competing and combinatory effects of chaotropes and kosmotropes will likely govern the habitability of the system (Pontefract *et al.*, 2017, 2019; Stevens and Cockell, 2020).

The formation of ice promotes cryoconcentration of the residual brine, as salts are efficiently excluded from the ice's crystal lattice structure (Feltham *et al.*, 2006; Hunke *et al.*, 2011), eventually saturating the brine and leading to the precipitation of salt hydrates. Although low temperatures

and brine saturation may limit habitability, both ice and hydrated salts are capable of entraining and preserving biomaterials (Pontefract *et al.*, 2017; Buffo *et al.*, 2019; Srivastava *et al.*, 2021), potentially providing a mechanism for long-term stasis of organisms when conditions become less favorable (Cosciotti *et al.*, 2019; Srivastava *et al.*, 2021).

1.2. Scientific motivation

The most promising worlds within our solar system that may harbor environments suitable for life all lie beyond the sun's habitable zone (*e.g.,* Europa, Enceladus, Mars, Ceres), precluding the long-term stability of liquid water on their surfaces (Marion *et al.*, 2003; Parkinson *et al.*, 2008; Tosca *et al.*, 2008; Priscu and Hand, 2012; Fox-Powell *et al.*, 2016; Castillo-Rogez, 2020; Castillo-Rogez *et al.*, 2020). As such, most high-priority astrobiology targets are situated beneath icy outer shells/regolith or occur as ephemeral/relict surface expressions of subsurface fluids.

In the case of Europa and Enceladus, this manifests in the form of global ice shells overlying regional or global subsurface oceans (Sotin and Tobie, 2004; Čadek *et al.*, 2016), with possible endogenic expression of ocean material through ocean-surface geophysical processes (Fig. 2) (*e.g.*, diapirism [Pappalardo and Barr, 2004; Nimmo and Pappalardo, 2006; Schmidt *et al.*, 2011], extensional band formation [Howell and Pappalardo, 2018], solid state convection [McKinnon, 1999; Barr and McKinnon, 2007; Weller *et al.*, 2019], fractures [Nimmo and Schenk, 2006; Walker *et al.*, 2014; Craft *et al.*, 2016; Nathan *et al.*, 2019], and plumes [Bauer *et al.*, 2010; Glein *et al.*, 2015; Sparks *et al.*, 2016]).

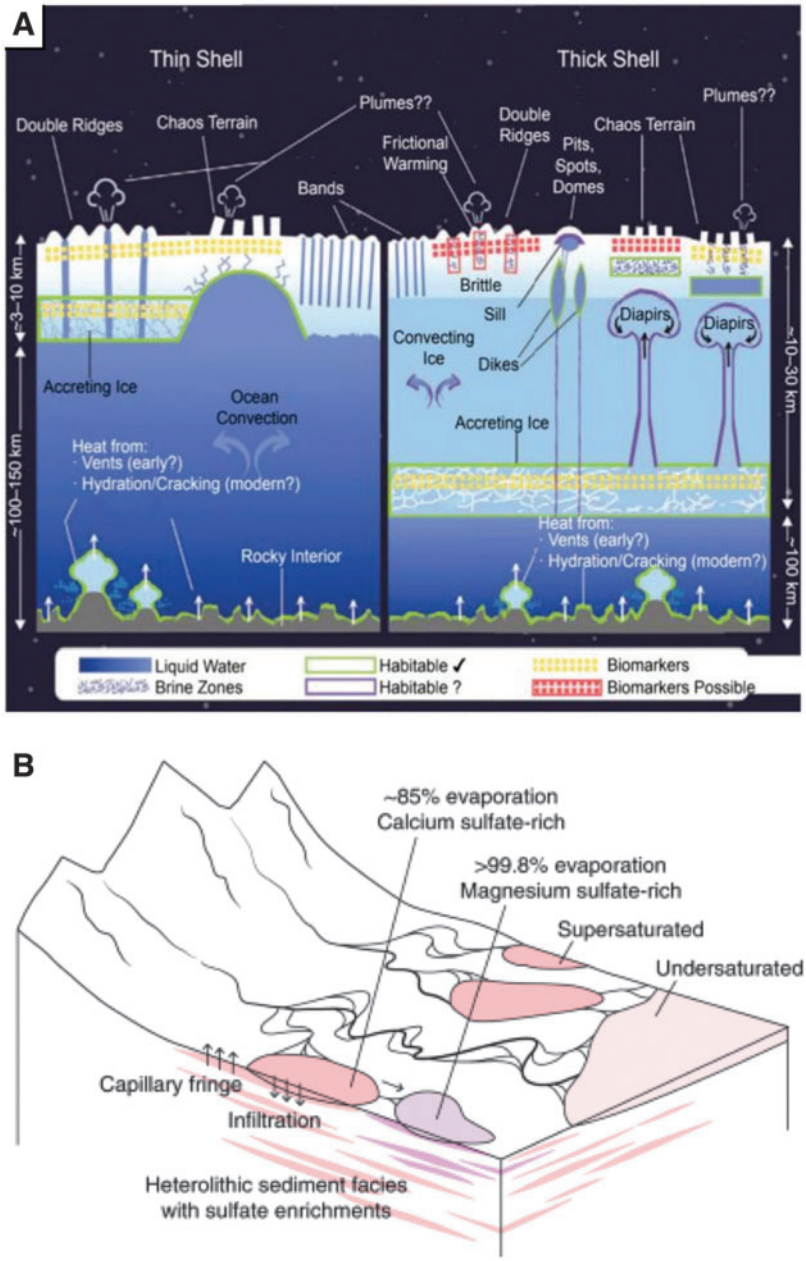

FIG. 2. Putative ice-brine environments on Mars and ice-ocean worlds. **(A)** The ice-ocean-seafloor system of Europa, highlighting the potential for ice shell hydrology driven by regional geodynamics. In addition to the global subsurface ocean, concentrated brine could facilitate stable hydrological features within the shell. Understanding their biogeochemical evolution is crucial to predicting their distribution, longevity, and habitability as well as linking shallow subsurface characteristics to underlying ocean properties. **(B)** Predicted fluvial and lacustrine dynamics in Mars' ancient Gale crater (Rapin *et al.*, 2019). Cyclic filling and evaporation of endorheic pools coupled with freezing surface temperatures could create environments that are strikingly similar to those found in the Canadian ice-brine systems investigated here (particularly their geochemical evolution and habitability). (Photo Credit: **A)** (Schmidt, 2020) **(B)** (Rapin *et al.*, 2019)).

For Mars it has been suggested that both historical and contemporary shallow subsurface brine systems and episodic surface expression of brine are responsible for the formation of fluvial and lacustrine geomorphological features (*e.g.,* Gale Crater—a potentially remnant analog to the Canadian lake systems investigated here; Fig. 2) and continue to interact with and are sourced from observed ground ice (Carr, 1987; Vaniman *et al.*, 2004; Zorzano *et al.*, 2009; Wray *et al.*, 2011; Toner *et al.*, 2014; Ojha *et al.*, 2015, 2020; Rapin *et al.*, 2019).

Further, subglacial hydrology in the Noachian era (Fastook and Head, 2015; Ojha *et al.*, 2020) and potential saline lakes beneath the present-day south polar layered deposit (Orosei *et al.*, 2018; Sori and Bramson, 2019; Grau Galofre *et al.*, 2020; Lauro *et al.*, 2021) may constitute additional habitable aqueous environments, suggesting that such systems could have existed in a number of regions in both Mars' past and present. Ceres may possess a contemporary deep brine reservoir, depending on the dwarf planet's interior geochemistry and thermodynamic evolution (Castillo-Rogez *et al.*, 2019), and both compositional and geologic measurements captured by the Dawn spacecraft suggest that a brine-rich melt lens was generated beneath Occator crater post-impact (Buczkowski *et al.*, 2019; Quick *et al.*, 2019; Schenk *et al.*, 2019; Scully *et al.*, 2019). With the unique link between water and life as we know it, identifying and improving our understanding of these ice-ocean/brine systems is imperative to future mission design in the lens of both planetary exploration and planetary protection.

A remaining hurdle exists in accessing and observing the underlying ocean/brine reservoir, as it frequently lies beneath meters or kilometers of ice. In the absence of *in situ* measurements, we rely on remote sensing techniques (*e.g.,* spectrographs, ice penetrating radar) to observe ice characteristics and relate these measurements to properties of the underlying liquid (Fanale *et al.*, 1999; Ojha *et al.*, 2015; Di Paolo *et al.*, 2016; Kalousova *et al.*, 2017; Orosei *et al.*, 2018). Fortunately, when ice forms it entrains biogeochemical signatures of its parent water reservoir and formation history (Kargel *et al.*, 2000; Buffo *et al.*, 2018, 2019, 2020).

On Earth, this entrainment has been observed in the salinity and bioburden profiles of both sea ice (Cox and Weeks, 1974; Nakawo and Sinha, 1981; Eicken, 1992; Cottier *et al.*, 1999; Thomas and Dieckmann, 2003; Loose *et al.*, 2011) and lake ice (Priscu *et al.*, 1998; Murray *et al.*, 2012; Santibáñez *et al.*, 2019).

Although the thermodynamics and biogeochemistry of ice formed from the Earth's sodium chloride (NaCl) rich ocean has been studied for nearly a century (Malmgren, 1927), the analogous processes in ices formed from more exotic ocean/brine compositions remain less constrained (exceptions being the ice covers of Antarctic dry valley lakes [Priscu *et al.*, 1998; Doran *et al.*, 2003; Murray *et al.*, 2012]). Exotic salt assemblages including magnesium, sulfate, and acid-bearing salts have been detected on Europa (Fanale *et al.*, 1999) and magnesium, sulfate, chlorate, and perchlorate salts are ubiquitous components of Mars' geology (Vaniman *et al.*, 2004; Tosca *et al.*, 2008; Ojha *et al.*, 2015; Pontefract *et al.*, 2017).

This is important, as it suggests that the oceans and brines of other solar system bodies may be quite different than the Earth's ocean (Kargel *et al.*, 2000; Zolotov and Shock, 2001; Zolotov, 2007; Toner *et al.*, 2014; Pontefract *et al.*, 2017). Likewise, the ice that forms in these planetary environments may have substantially varied characteristics (*e.g.,* microstructure, biochemistry, strength, viscosity). Differing chemistries could drastically impact the habitability and geophysics of ice-ocean/brine worlds on both local and global scales and affect the relationship between ice characteristics and interior reservoir properties and dynamics—an imperative for the interpretation of spacecraft observations.

Fortuitously, the hypersaline lakes of British Columbia provide a natural laboratory in which to observe the thermophysical and biogeochemical evolution of ices formed from compositionally diverse analog brines (Renaut and Long, 1989; Fox-Powell and Cockell, 2018). Further, the magnesium sulfate ($MgSO_4$) and sodium sulfate (Na_2SO_4) dominated chemistries of these lakes mirror the predicted ocean/brine compositions of both icy satellites (Zolotov and Shock, 2001; Zolotov, 2007) and Mars (Vaniman *et al.*, 2004; Toner *et al.*, 2014; Pontefract *et al.*, 2017).

Cumulatively, observations of the thermal, structural, and biogeochemical profiles of British Columbia's diverse hypersaline lakes provide a method to assess the spatiotemporal habitability and biosignature distribution of unique ice-brine analog systems. This not only has far-reaching implications for extremophilic adaptation and the limits of life on Earth but also provides an ideal system to investigate the thermophysical evolution and hypothetical biogeochemical dynamics of analogous planetary ice-brine environments while providing a benchmark to validate models designed to simulate these systems (Buffo *et al.*, 2019, 2021b; Brown *et al.*, 2020b).

In Section 2, we describe our field and laboratory methods for the acquisition and analysis of ice and brine samples recovered from five hypersaline lakes in south central British Columbia. In Section 3, we present our results, which include thermal, physical (porosity, permeability), chemical (ionic composition), and biological (cell density) characterizations of the ice covers and brines of these unique analog systems. In Section 4, we discuss the novel properties and dynamics observed in the lakes and the implications this work has for improving our understanding of planetary ice-brine systems.

2. Methods

Five lakes were visited during two field campaigns (February 2019 and February 2020): Basque Lake 1 (50.60012°, −121.35967°), Basque Lake 2 (50.59336°, −121.34974°), Basque Lake 4 (50.58867°, −121.34317°), Last Chance Lake (51.32775°, −121.63576°), and Salt Lake (51.07298°, −121.58441°) (Fig. 3). Basque Lakes 1, 2, and 4 as well as Salt Lake are $MgSO_4$-dominated systems, whereas Last Chance Lake is a Na_2SO_4 and sodium carbonate (Na_2CO_3) dominated system.

At each of the five lakes, sample sites ($n = 1$–3) were selected to represent diverse locations within the lake, located either within discrete brine pools, or as edge to center transects when pools could not be identified due to high lake levels (leading to subaqueous pools). At each site, the thickness of the ice and underlying brine layer was

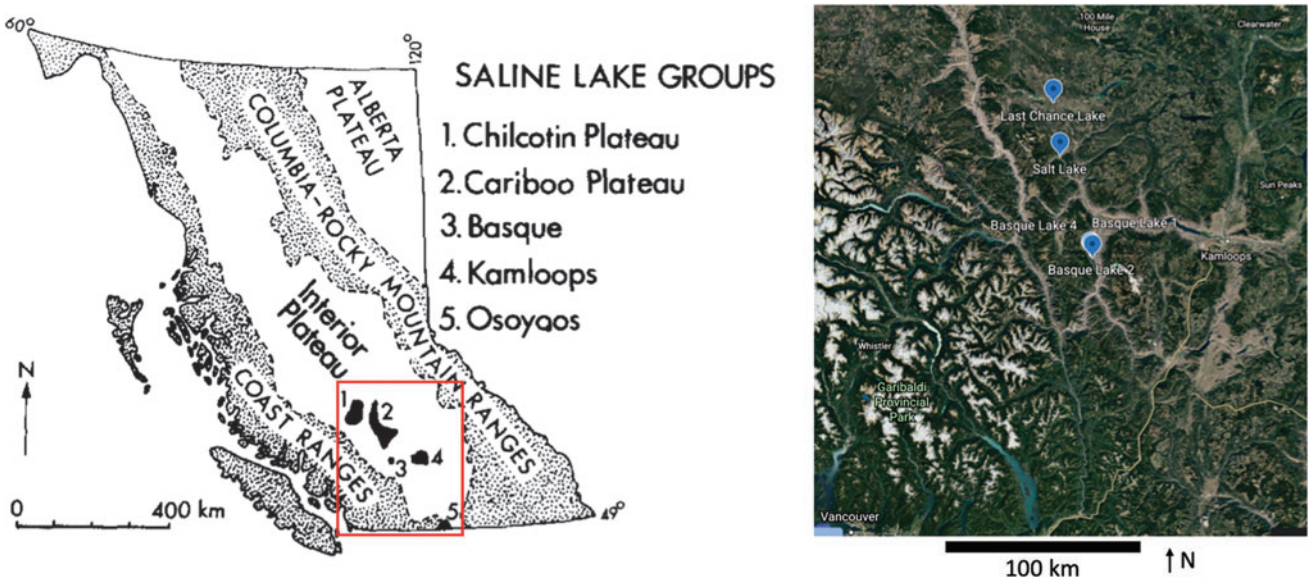

FIG. 3. Hypersaline lake locations. (Left) Map of the hypersaline lake groups of central British Columbia (modified from [Renaut and Long (1989)]). Last Chance Lake and Salt Lake are members of the Cariboo Plateau group whereas Basque Lakes 1, 2, and 4 are members of the Basque group. (Right) Enlarged view of the region outlined in red showing the lake locations visited during February 2020.

measured (Section 3.2). When present, precipitated salt at the base of the brine layer was also measured. Ice cores were extracted from descending sections of the ice column by using a carbide-tipped 1–1/4″ hole saw drill bit (Fig. 4C) and stored in sterile amber Nalgene bottles.

A temperature profile was taken by using a probe thermometer with a precision of 0.01°C as the cores were removed, and brine was extracted from the underlying pool/lake with a sterilized syringe if the ice was not frozen to the underlying sediments (Fig. 4C and Section 3.3.1). These ice cores and brine samples were used to derive the ionic composition and bioburden profiles of the lake ice-brine systems (Section 3.4). In addition, long-term temperature loggers that had been deployed in September 2019 to observe seasonal variations in brine and air temperature were recovered in February 2020 (Section 3.3.2).

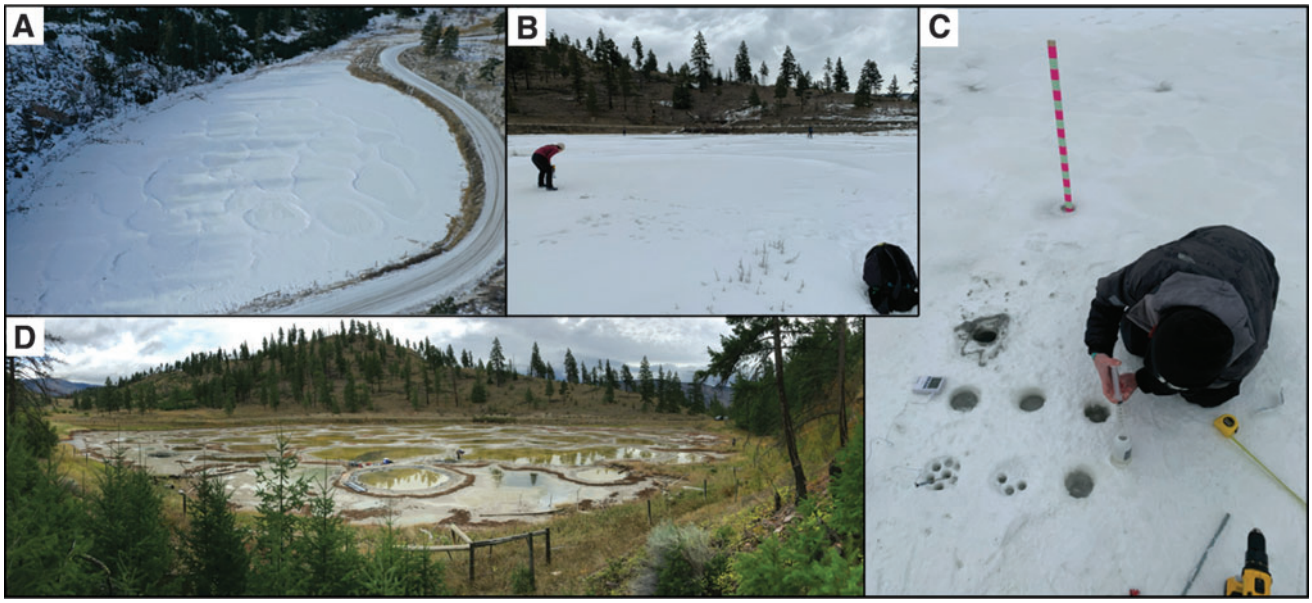

FIG. 4. Field work at Basque Lake 2. **(A)** Drone image of Basque Lake 2 taken in February 2019. The segregated brine pools, more evident in **(D)**, can still be seen under the snow cover. **(B)** Ground photo of a sample site as we begin to drill the borehole array seen in the next panel. **(C)** The typical sampling procedure where ice thickness and temperature are recorded, ice cores are gathered, and brine is extracted from the underlying lake. **(D)** The lake without an ice cover, photographed in September 2019 (taken from hillside at top left of image **A**).

The HOBO temperature loggers recorded data hourly and were placed at Basque Lake 2 and Last Chance Lake, with one logger positioned directly above the sediment layer in a chosen pool, another in the middle of the water column, and a third logger placed around the lake to gather surrounding air temperature. Finally, brine infill experiments were conducted to assess ice permeability. To do this, ''sackholes'' were drilled to different depths within the ice cover and allowed to fill with brine via percolation through the underlying porous ice. By measuring the rate at which the brine infills the hole, the permeability of the ice beneath the hole can be estimated (Section 3.5) (Freitag and Eicken, 2003).

To prepare the samples for biological and chemical analysis, the ice samples were melted in a hot water bath within 18 h of collection, and then both ice and brine samples were split for two workflows. One split involved aliquoting 45 mL of the unfiltered sample to a 50 mL Falcon tube and adding 2.5% glutaraldehyde to a final concentration of 0.25% to fix the cells for bioburden analysis. From that, 2 mL of the fixed solution was aliquoted into a cryotube for cell counting via flow cytometry.

All samples were then frozen at −20°C and shipped frozen to either Scripps Institution of Oceanography (cryotubes) or Georgia Institute of Technology (Falcon tubes). Cell counts were acquired using two techniques: (1) staining the cells with 4′,6-diamidino-2-phenylindole (DAPI) and imaging them using a Zeiss Epifluorescent Microscope (see Supplementary Material Section S1 for methods and Supplementary Figure S1) and (2) flow cytometry (Section 3.4) following the methods of Klempay *et al.* (2021): In brief, fixed samples were stained with SYBR Green I nucleic acid dye (Molecular Probes) and spiked with a known quantity of 123count eBeads counting beads (Thermo Fisher).

Samples were then run on a Guava easyCyte HT flow cytometer (Luminex). Flow cytometry outputs were analyzed in R using the flowCore library (Ellis *et al.*, 2009) and custom scripts.

For the second split, we filtered the remaining sample (ice or brine) through a 0.2 µm polyethersulfone membrane Sterivex filter (filters were saved [frozen at −20°C] for future work that will assess the community composition of these systems as part of the larger Oceans Across Space and Time project). The filtrate was then frozen at −20°C and cold shipped to ALS Environmental in Tucson, Arizona for chemical analysis via ion chromatography (IC) and ion coupled plasma mass spectrometry (ICP-MS) methods. Samples were analyzed for the following ions: Br, Cl, F, NO_3, SO_4, CO_3 (alkalinity), Ca, Mg, K, and Na (Section 3.4) as well as total dissolved solids, pH, density, and conductivity.

3. Results

3.1. Physical properties of the ice

The ice cover of the lakes visited in both field campaigns was characterized by porous, soft, cloudy/bubbly ice that was frequently damp with brine in all but the coldest ambient sampling temperatures. The ice crystals had a lamellar structure similar

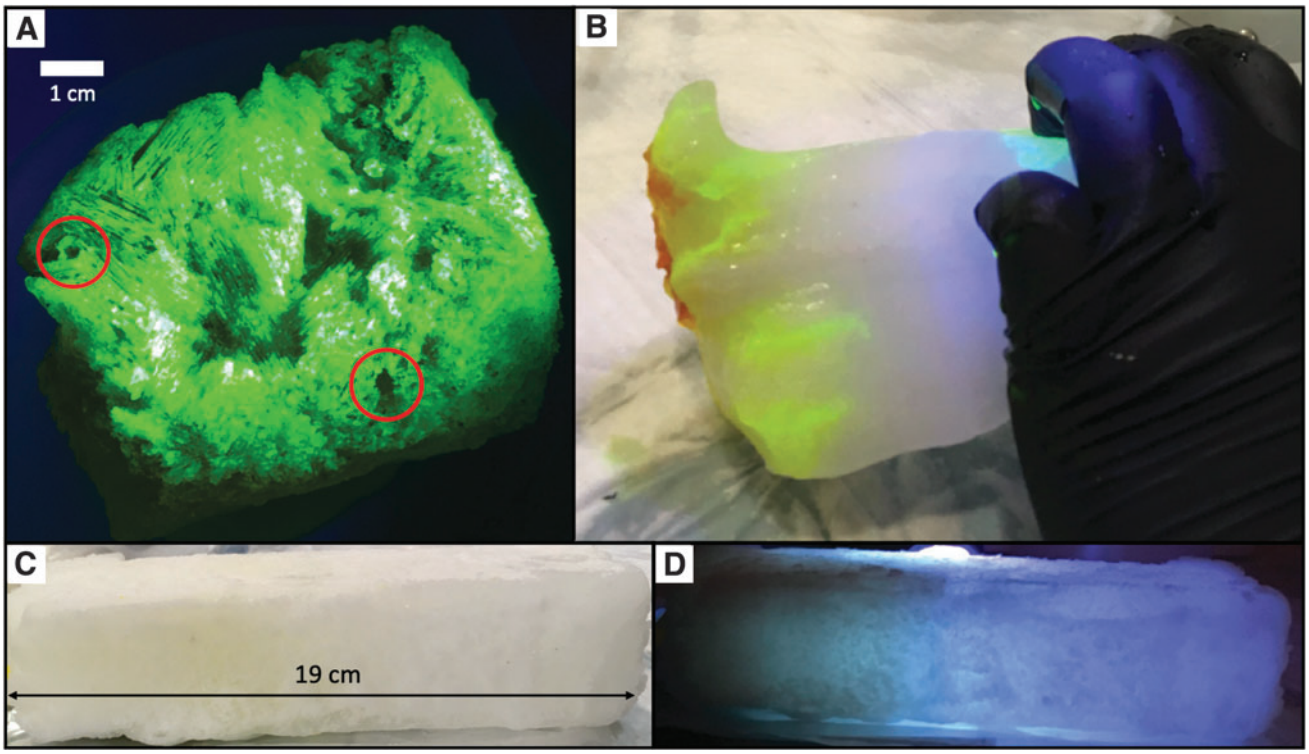

FIG. 5. Structural properties of Cariboo Plateau lake ices. **(A)** Lamellar crystal structures at the base of an ice core from Salt Lake (February 2019). A fluorescein solution was poured onto the base of the inverted ice core and it was illuminated with a UV flashlight. The openings of two brine channels are circled in red. **(B)** Brine channels in the basal layer of the Salt Like ice core pictured in frame **(A)**. We melted the edges of the ice core away by running it under water, revealing locations where fluorescein had percolated into the ice core via brine channels (again, illuminated by a UV flashlight). **(C)** Salt Lake ice core before fluorescein was added (visible light). The bottom of the core is to the left of the image. **(D)** Same as **(C)** under UV illumination. Autofluorescence is evident near the base of the ice core, indicating the presence of microorganisms. UV = ultraviolet.

to that of columnar sea ice (Fig. 5A). The random orientation of the crystals is indicative of growth under quiescent conditions, as expected for endorheic basins with limited flow. On drilling, the ice was noticeably odorous (sulfur scented), an aspect that increased with depth, consistent with measurements indicating that substantial amounts of volatiles were entrained within the ice cover (Supplementary Fig. S3). The basal portion of the ice cover (~5 cm) possessed visible brine channels (Fig. 5B) similar to those seen in sea ice.

These high porosity dendritic conduits are the byproduct of density-driven convective overturn in the lower layers of the ice (Notz and Worster, 2009). In other systems where brine channels are observed, this convective overturn proceeds as follows: As an ocean/brine freezes, salts are rejected from the forming ice lattice, producing a porous ice matrix saturated with hypersaline interstitial brine (a ''mushy layer'' [Feltham *et al.*, 2006]). Where the porous ice matrix is permeable enough to sustain Darcy flow (fluid flow in a porous medium [Bear, 2013]), the cold, saline, dense fluid at the top of the mushy layer downwells into the underlying fluid reservoir, forming (dissolving) brine channels. The resultant porous basal layer of ocean/brine-derived ices can sustain substantial thermochemical gradients that can provide metabolic energy sources to any resident organisms (Loose *et al.*, 2011). In sea ice this layer supports a substantial biological community, including primary producers that are essential to the polar oceans (*e.g.,* ice algae), grazers, bacteria, and macrofauna (Loose *et al.*, 2011; Tedesco and Vichi, 2014).

Similarly, on ultraviolet irradiation, an ice core extracted from Salt Lake during the February 2019 season exhibited visibly enhanced autofluorescence in the region adjacent to the ice-brine interface (Fig. 5C, D), suggesting an amplified presence of microbiota when compared with the upper portion of the ice cover. This is corroborated by the quantitative biological profiles of Section 3.4.

3.2. Stratigraphy of the ice-brine lake systems

During the winter, most of the lakes possess four primary layers: (1) an ice cover, (2) a shallow (<1 m thick) brine layer, (3) solid salt hydrates (Supplementary Fig. S2), and (4) underlying sediments. Stratigraphic profiles of 12 sample sites visited during February 2020 can be seen in Fig. 6. Most sites have the expected ice → brine → salt hydrate → sediment vertical layering that occurs when salts are rejected from the forming ice cover, saturate the underlying brine, and precipitate out of solution, forming a salt hydrate layer atop the underlying sediments.

However, there are a number of interesting exceptions as well as additional layering features that may provide further insight into the physical and geochemical evolution of these systems. Typically, deeper lakes are fresher and thus may not reach their saturation points during winter (*e.g.,* Salt Lake—note the limited freezing point depression of the sub-ice brine; Fig. 7). An exception is Basque Lake 1 sample Site 3, which possessed a salt hydrate layer suggesting that the lake brine is saturated; this is reasonable given the extremely low temperature of the brine (Fig. 7).

Other interesting features include: (1) an intra-ice brine layer observed in the ice cover of Basque Lake 2 sample Site 2 that may be indicative of eutectic melting in the ice or over pressurization of the underlying brine (if progressive freezing is not compensated by ice uplift); (2) the alternating layers of salt and sediment at Basque Lake 4 sample Site 2, indicating localized salt precipitation features (note the lack of a salt layer for Basque Lake 4 sample Site 1) that are likely the remnant ''crystal bowls'' (Renaut and Long, 1989) of previously existing brine pools (see Fig. 2 of Foster *et al.* [2010]); (3) the confirmed existence of a substantial salt basement beneath the lakes (*e.g.*, Basque Lake 4 sample Site 2—in many cases, there likely exists a salt hydrate basement beneath the lowest sediment layer measured [Jenkins, 1918; Renaut and Long, 1989]); (4) two visibly distinct salt hydrate layers at the base of Last Chance Lake (a 1 cm layer overlying a 5 cm layer; Supplementary Fig. S2). The geophysical and biogeochemical implications for both terrestrial and planetary environments are discussed in Section 4.

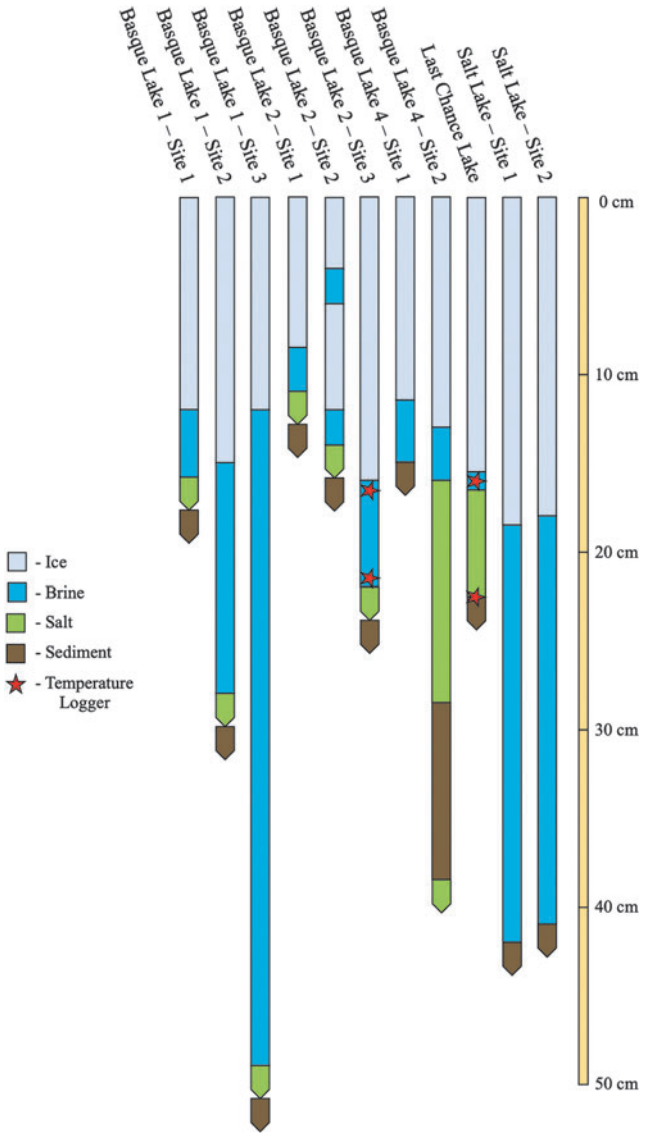

FIG. 6. Stratigraphic profiles of select February 2020 sample sites. Portions of the profiles represented by bars with squared ends have known thicknesses. Portions of the profile with pointed ends have unknown thicknesses (they were either too thin to measure, too thick to extract, or the lowest layer accessed).

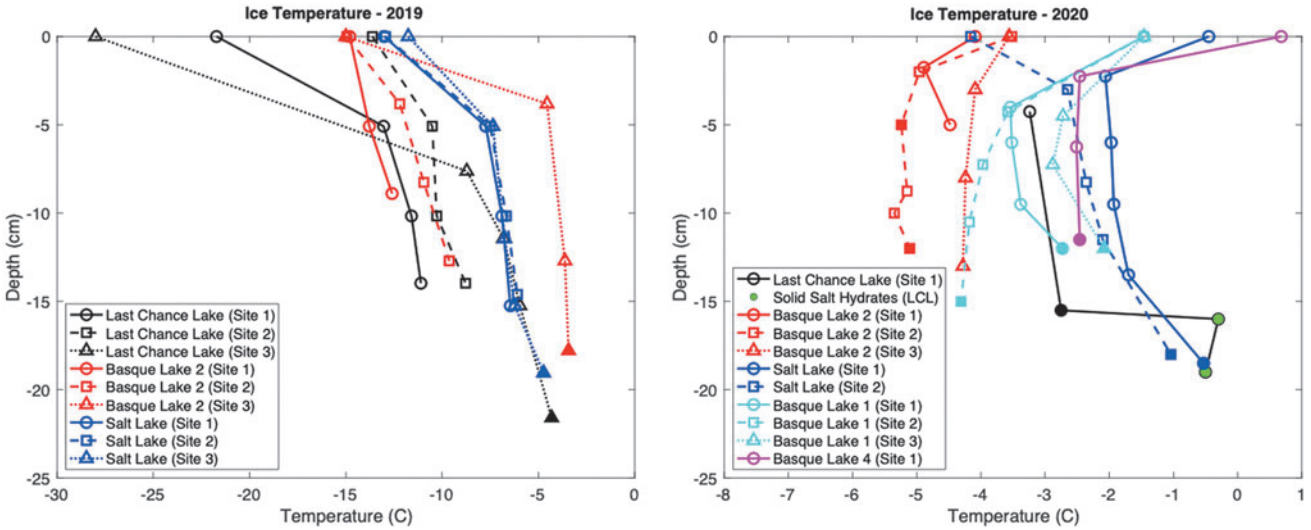

FIG. 7. Ice cover temperature profiles. (Left) Vertical ice core temperature profiles taken during February 2019. Filled symbols signify a brine temperature. (Right) Vertical ice core temperature profiles taken during February 2020. At Last Chance Lake, two distinct salt hydrate layers had precipitated just above the lake sediments. Note the unique interior brine layer at the Basque Lake 2 Site 2 location. (Note: probe thermometer precision is 0.01°C).

3.3. Temperature profiles

We acquired two distinct temperature datasets during our 2019 and 2020 February field campaigns. The first consists of vertical temperature profiles for all extracted ice cores. The second consists of hourly air and brine temperature records from September 2019 to February 2020, obtained with HOBO temperature sensors.

3.3.1. Ice core temperatures. Ice and brine temperature profiles for all sites visited in 2019 and 2020 can be seen in Fig. 7. Due to consistently colder ambient air temperatures (Fig. 7; 0 cm), the temperature profiles for the 2019 ice covers are much more monotonic, where temperatures increase with depth—profiles lacking brine measurements entirely indicate ponds that were frozen to the sediment bed. Conversely, high daytime temperatures during February 2020 can be seen warming the near surface ice, in many cases to values that exceed the temperatures deeper in the ice column.

Profiles without brine measurements are frozen to the sediment bed. Brine temperatures ranged from −5.31°C to −0.53°C and are significantly below the freezing point of fresh water due to the presence of dissolved salts (Section 3.4). An inter-ice brine layer (∼0.5–2 cm thick) was observed at Basque Lake 2 sample Site 2 in February of 2020 (Fig. 7; filled red square at ∼5 cm). This unique feature has important implications for the potential generation of brines in the icy regolith of Mars and ice shells of ice-ocean worlds.

We discuss potential formation mechanisms for the layer as well as its astrobiological relevance in Section 4. It is not uncommon for salt hydrate layers to occur at the base of the lakes (Section 3.2); however, the extraction of these layers through holes in the ice cover is far from straightforward. With strengths and hardnesses that exceed those of ice (Durham *et al.*, 2005), even thin layers (∼6 cm) must be chiseled through.

In 2020 at Last Chance Lake sample Site 1, the wooden stake holding the HOBO temperature sensors was firmly encased by the salt hydrate layer at the base of the lake, with one temperature sensor attached to the stake below the hydrate layer (see Fig. 6 and Section 3.3.2). To extract the temperature sensor, the hydrate layer was chiseled through with a hammer and metal rod (Supplementary Fig. S2). Exceptionally warm temperatures (−0.3°C and −0.5°C) were measured in both the distinct hydrate layers described in Section 3.2 (green circles of Fig. 7). The potential importance of salt hydrates in these and analogous planetary ice-brine systems is discussed in Section 4.

3.3.2. Seasonal temperatures. During September 2019, six HOBO temperature loggers were installed at the hypersaline lakes (three at Last Chance Lake, three at Basque Lake 2). At each lake, one temperature logger was attached to a nearby tree to measure air temperature. The other two loggers were affixed to a wooden stake with zip ties and driven into the sediments of a brine pool. One logger was placed near the brine-sediment interface, and the other was placed in the middle of the water column. Between September 2019 and February 2020, the loggers recorded hourly temperature readings, the results of which can be seen in Fig. 8. At the time of extraction, both temperature loggers were in the sub-ice brine layer of Basque Lake 2.

At Last Chance Lake, one temperature logger was in the sub-ice brine layer, and the other was beneath a 6 cm layer of precipitated salt hydrates (see Fig. 6 for exact locations). During the fall, large diurnal variations in temperature occur in both the air and brine. On the formation of an ice cover in late November, the brine becomes extremely well insulated and no longer varies appreciably on a diurnal scale. The minimum brine temperatures recorded were −6.37°C (December 1) and −8.45°C (November 30) for Basque Lake 2 and Last Chance Lake, respectively.

The subsequent warming of the brines and a lack of any appreciable temperature variations after the brines reached their minimum temperatures (even under substantial cooling

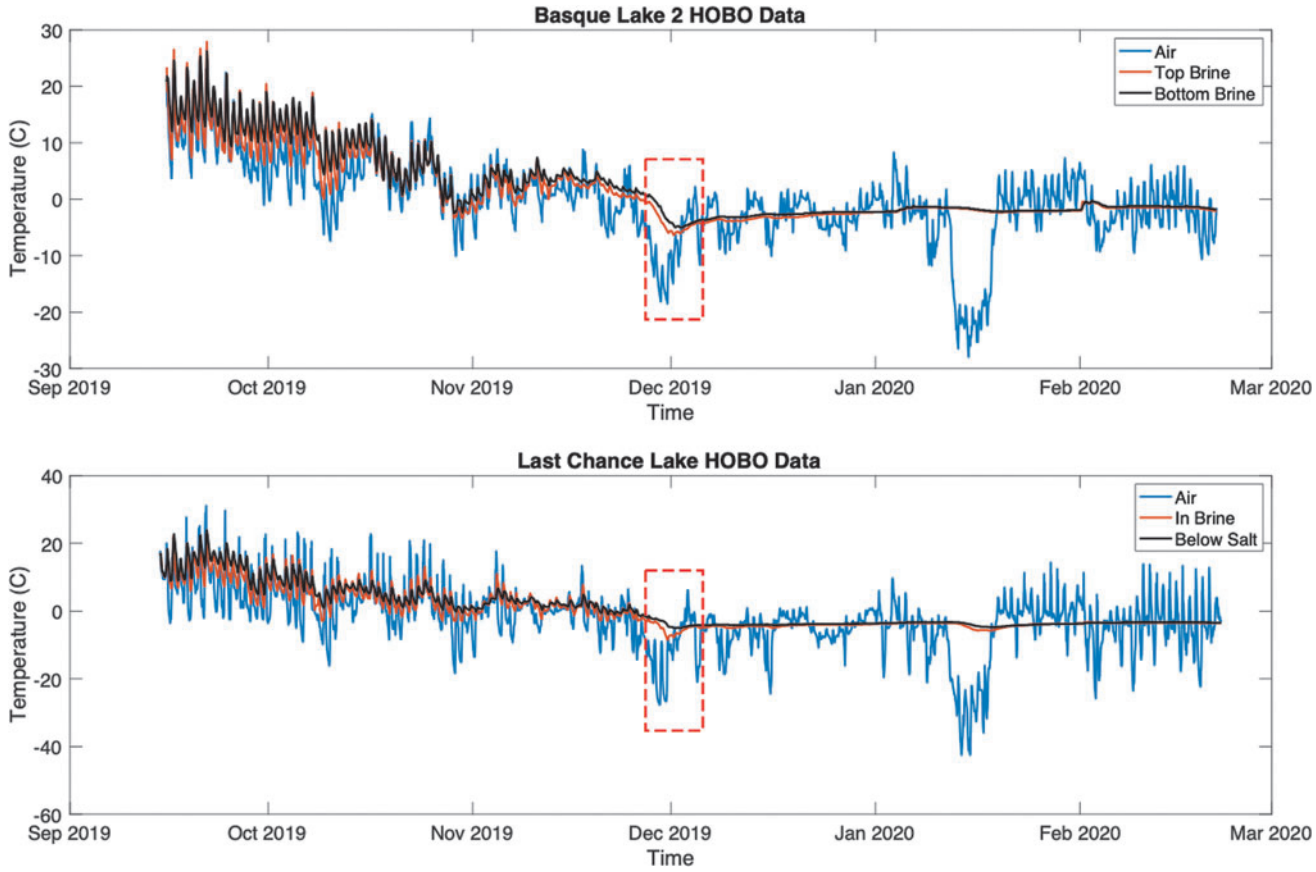

FIG. 8. Seasonal variations in air and brine temperatures. (Top) Hourly temperature data for Basque Lake 2. (Bottom) Hourly temperature data for Last Chance Lake. (Red boxes highlight early season brine temperature minimums and subsequent brine warming, which are potentially indicative of brine supercooling and latent heat release due to salt hydrate precipitation, respectively).

that occurred mid-January) suggests significant insulation by the overlying ice, a substantial heat source due to salt hydrate precipitation in the underlying brine, or both.

An early season minimum brine temperature followed by a significant temperature increase (red boxes, Fig. 8) favors the presence of the latter, as it appears that the brine becomes supercooled, precipitates salt hydrates, and then remains at or near its eutectic temperature (no longer requiring supercooling/supersaturation to nucleate salt hydrates as a substrate already exists for continued precipitation [Toner *et al.*, 2014]). Further discussion of this process and its relevance to both terrestrial and planetary ice-brine systems is included in Section 4.

3.4. Major ion and bioburden profiles

Bioburden and chemical profiles from each lake were derived by using IC, ICP-MS, fluorescence microscopy, and flow cytometry. The vertical distributions of major ions in each lake (ice cover and underlying brine) are shown in Fig. 9. All three of the Basque Lakes sampled (1, 2, and 4) as well as Salt Lake were dominated by sulfate, with the second most abundant ion being magnesium. Last Chance Lake was dominated by carbonate, sodium, chloride, and sulfate with a negligible concentration of magnesium. Basque Lake 2 had the highest ionic concentration of all the lakes.

The ion speciation trends observed in the lakes are consistent with previous investigations (Renaut and Long, 1989), whereas ionic concentrations vary from historical measurements. The latter can be attributed to shallow lake depths and seasonally/annually variable precipitation, evaporation, dissolution, and freezing/melting cycles—processes that continuously dilute and concentrate the residual brine.

A number of the ion profiles have ''c-shaped'' distributions, with high ion content in the near surface ice, lower ion content in the middle portion of the ice column, and increasing ion content approaching the base of the ice column and underlying brine, similar to the characteristic bulk salinity profile of first year sea ice (Malmgren, 1927; Eicken, 1992). The amplifications near the surface are due to rapid freezing, as heat is lost to the colder atmosphere before salt can be rejected into the underlying fluid.

Amplifications near the base of the ice are due to the ice-brine interface existing as a porous two-phase layer, composed of a solid ice matrix bathed in concentrated interstitial brine—a ubiquitous feature of ice formed from saline solutions (Feltham *et al.*, 2006; Buffo, 2019). A number of exceptions to the ''c-shaped'' trend exist in our observations: (1) exceptionally low ion contents in the shallow ice of Salt Lake (Fig. 9A), which we have reason to believe is due to analysis error, as the reported ion concentrations

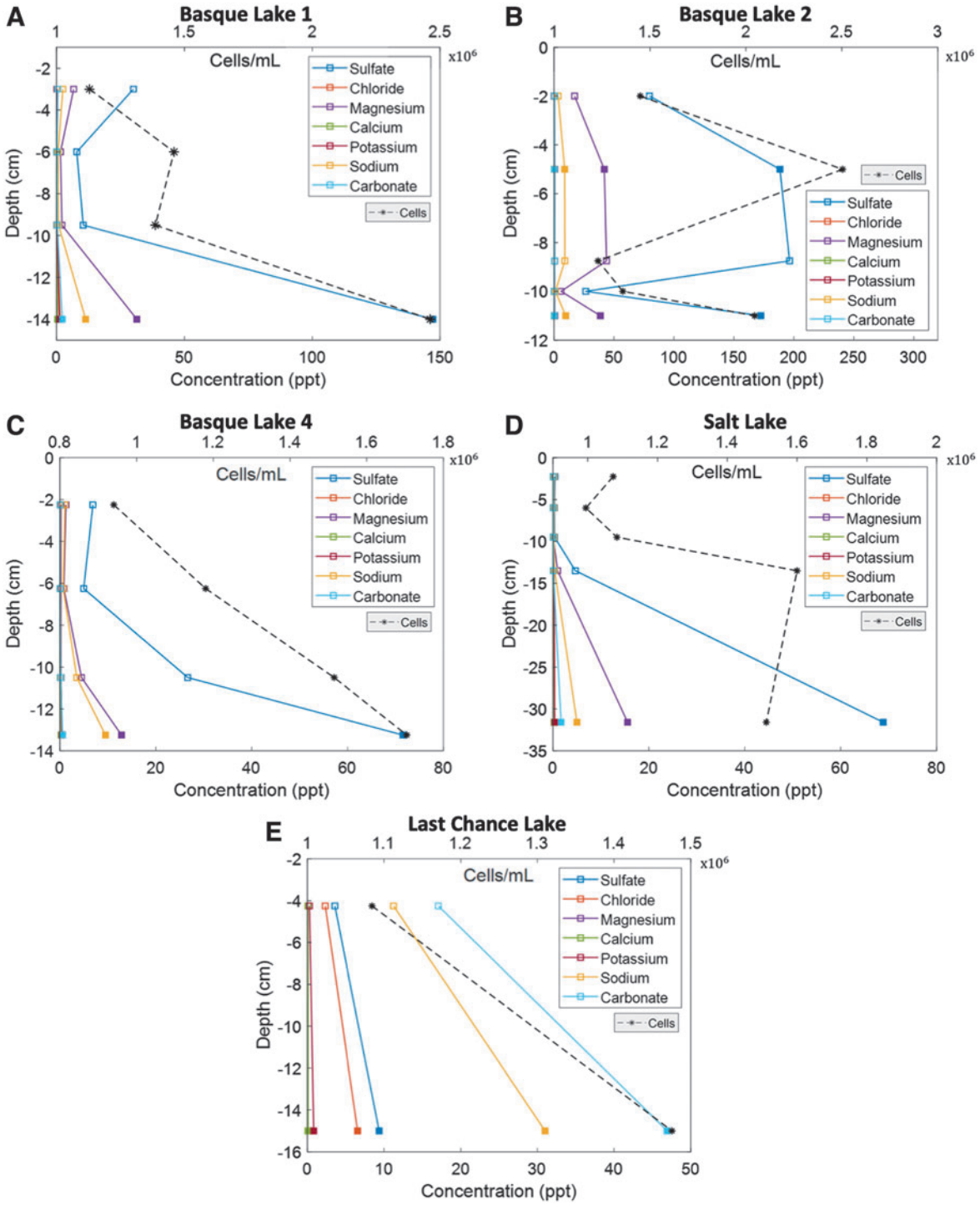

FIG. 9. Major ion and cell density profiles of selected lake sites. **(A)** Basque Lake 1—exhibiting a ''c-shaped'' ionic profile and a general increase in cell density as the ice-brine interface is approached. **(B)** Basque Lake 2—with amplified salt and cell concentrations in the internal brine layer ∼5 cm below the surface, even exceeding those of the underlying brine. Basque Lake 2 is the most concentrated lake of the Basque Lakes sampled and contains a higher cell density in the top ice layer than the other lakes. **(C)** Basque Lake 4—similar to Basque Lake 1, Basque Lake 4 exhibits a ''c-shaped'' ionic profile and a trend of increasing cell density with depth. Basque Lake 4 has a lower $MgSO_4$ concentration and lower cell density in its underlying brine than the other Basque Lakes. **(D)** Salt Lake—there exists a spike in cell density in the bottom ice sample, around −13.5 cm, exceeding that of the brine sample at −32 cm. **(E)** Last Chance Lake—only one ice sample was obtained during February 2020 due to warm temperatures. Last Chance Lake is the only Na-CO_3 rich lake sampled and has the lowest cell density in its underlying brine. All ionic concentration and cell density values can be found in Supplementary Tables S1 and S2, respectively (Note: filled symbols represent brine samples). $MgSO_4$ = magnesium sulfate.

are not charge balanced; (2) only one ice sample from Last Chance Lake was acquired due to exceptionally warm temperatures (deeper ice had excessive brine infill and could not be adequately cored without contamination from the infilling brine); and (3) an internal brine layer existed in the ice cover of Basque Lake 2 (Fig. 6), which exhibited exceptionally high ion concentrations (and cell densities).

Vertical microbial cell density distributions for all the lakes are shown in Fig. 9. Cell densities tend to increase with depth—with the notable exception of Basque Lake 2—which features an inter-ice brine layer. This inter-ice layer was located 5 cm below the surface and contained almost twice the cell concentration (2.503×10^6 cell/mL) as the three other depths measured in the ice cover (1.449×10^6, 1.229×10^6, and 1.358×10^6 cell/mL).

Salt Lake had a noticeable peak of cell density at a depth of 13.5cm, which then decreased slightly in the subsequent brine layer. Last Chance Lake had the lowest basal brine cell density. The geophysical and astrobiological implications of the observed cell densities and major ion distributions are discussed in Section 4.

3.5. Permeability

One of the primary controls of fluid and solute transport in ocean and brine derived ices (*e.g.,* sea ice) is the permeability of the ice cover. Desalination of the ice, through both gravity drainage and surface flushing, depends critically on the flow of brine and meltwater through the ice, and in turn governs the resultant salinity distribution in the ice (Notz and Worster, 2009). In high porosity (generally highly permeable) regions near the ice-ocean interface, nutrient and detritus transport is a crucial process governing the productivity and sustainability of biological communities that thrive in the interstitial brine (Thomas and Dieckmann, 2003; Loose *et al.*, 2011).

It stands to reason that fluid transport, and thus permeability, likely plays an equally important role in the biogeochemical evolution of the hypersaline ice-brine systems investigated here.

In February 2020, it was relatively warm (air temperatures exceeded 0°C by mid-morning) the day Last Chance Lake was sampled. Ice cores were extracted at one site; however, by the time a second site was selected, rapid brine infill into boreholes of all depths precluded coring as inflowing brine from the underlying reservoir would contaminate ion and bioburden estimates. Taking advantage of the highly porous ice, we conducted three slug test experiments (borehole depths of 6, 8, and 10 cm) to investigate the permeability of the ice cover, the results of which can be seen in Fig. 10.

These recovery curves track the hydraulic head of the brine infilling the borehole over time. Here, hydraulic head is equivalent to the difference between the height of the infilling brine and the freeboard level. This is a common technique used in sea ice research, and it can be shown that the temporal evolution of the hydraulic head is related to permeability via Freitag and Eicken (2003):

$$h(t) = h(t_0) \exp\left(-k \frac{g\rho t}{\eta L} \right) \quad (1)$$

where $h(t)$ is the hydraulic head at time t, $h(t_0)$ is the hydraulic head at the onset of the slug test, k is permeability, g is gravity, ρ is brine density, η is the dynamic viscosity of the brine, and L is the distance between the bottom of the borehole and the base of the ice cover.

Best fit curves of this functional form have been applied to all three slug test experiments and can be seen plotted against the data in Fig. 10. Our measurements are well represented by the decaying exponential of Equation 1. As borehole depth increases, the quality of the fits decreases.

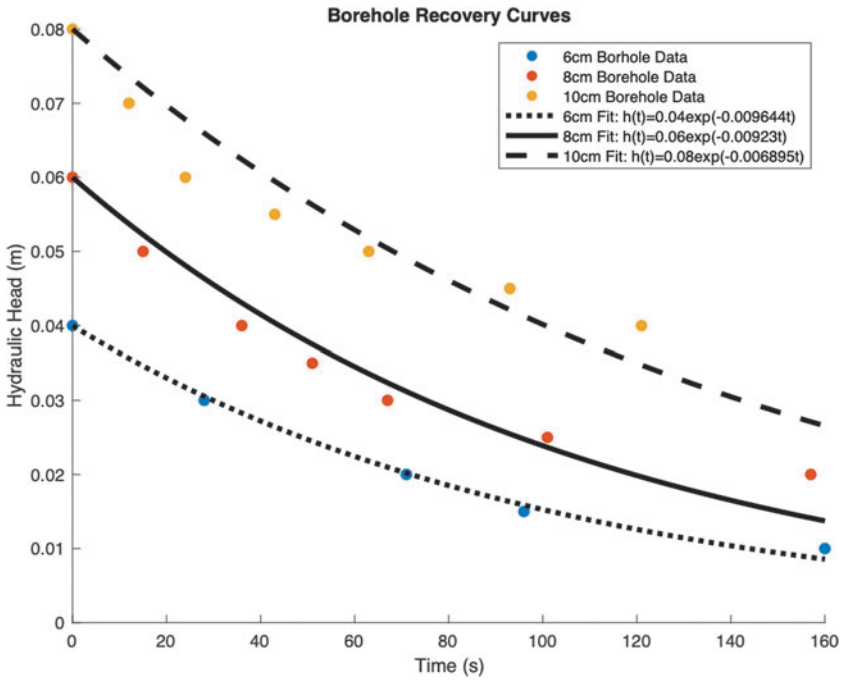

FIG. 10. Slug test recovery curves used to estimate ice permeability. Temporal variations in hydraulic head are measured as brine infills three boreholes of a different depth (6, 8, and 10 cm from the ice surface). Exponential decay curves (Eq. 1) are fit to the hydraulic head measurements (based on the method presented in Freitag and Eicken [2003]).

This is likely due to increased lateral brine infiltration in deeper boreholes. Equation 1 assumes only vertical brine infiltration from the base of the borehole. Although this is likely the main source of brine infiltration, the sides of the borehole will also experience a nonzero amount of lateral infiltration. Deeper boreholes have larger sidewall surface areas and, thus, will be more affected by this process. Typically, studies implementing the slug test technique will deploy a hollow cylindrical casing to minimize the effects of lateral brine infiltration. The impromptu nature of our study left us wanting in this regard and would have likely reduced the amount of misfit in our deeper borehole measurements.

Nevertheless, we can use the exponential coefficients of our fit lines and Equation 1 to acquire upper bound estimates of the ice permeability. The permeabilities of the 6, 8, and 10 cm boreholes are $1.6\times10^{-10}\,m^2$, $1.2\times10^{-10}\,m^2$, and $6.3\times10^{-11}\,m^2$, respectively. There is a slightly decreasing trend in permeability with depth, which could correlate to enhanced porosities in the rapidly cooled, near surface ice (Buffo *et al.*, 2018).

As the ice-brine interface is approached, permeabilities increase dramatically, evidenced by boreholes drilled below 10 cm infilling with brine too rapidly to accurately measure the change in hydraulic head. The estimated permeabilities of the Last Chance Lake ice fall in the center of permeabilities observed in natural and laboratory grown sea ice, which range from $10\times10^{-13}\,m^2$ to $10\times10^{-7}\,m^2$ (see Fig. 7a of Freitag and Eicken [2003]).

3.6. Porosity

Permeability is largely driven by porosity (ϕ), which plays an important role for both thermophysical and biogeochemical processes in ice-brine systems. Porosity, or liquid fraction, aids in facilitating solute (*e.g.,* salts, nutrients, waste) transport throughout the ice via connected brine networks. Similar to sea ice, higher porosity regions will likely be associated with amplified fluid flow, whereas low porosity regions should limit fluid flow and trap brines in discrete brine pockets as flow networks become more disconnected on continued solidification (Golden *et al.*, 1998, 2007).

The complex microstructure of saline ices, coupled with their physical and thermal fragility, makes direct measurements of ice porosity quite challenging in the field. Even in laboratory settings, the utilization of microcomputed tomography methods to measure ice porosity must carefully control the temperature of the sample to avoid melting, freezing, and redistribution of the fluid phase (Golden *et al.*, 1998, 2007; Maus *et al.*, 2020). Fortunately, there exists a link between the temperature, ionic composition, and liquid fraction of a solution.

Conceptually similar to the eutectic phase diagrams of simpler binary or ternary solutions, equilibrium and fractionation chemistry models (*e.g.*, FREZCHEM [Marion *et al.*, 1999] PHREEQC [Parkhurst and Appelo, 1999, 2013], SeaFreeze [Journaux *et al.*, 2020]) are able to utilize Pitzer equations or Gibbs free energy approaches to predict the composition and phase evolution of a solution as it is frozen.

Here, we use PHREEQC, our *in situ* ice temperature measurements (Section 3.3.1), and our ionic concentration measurements (Section 3.4) to estimate the porosity (liquid fraction) of the ice covers (Fig. 11). The colder atmospheric temperatures present during February 2019 result in low porosities (0.008–0.086) and porosity profiles that generally increase with depth. Conversely, the warm surface temperatures during the February 2020 campaign result in higher overall porosities (0.019–0.227), particularly in the warm shallow ice layers, likely due to melting/dissolution of the ice.

This link between warm surface temperature and high porosities may provide an explanation for the brine layer observed at Basque Lake 2. If the shallow ice were warmed to a point where solutes could be mobilized in the pore space of the ice (*e.g.,* by air temperatures >0°C; Fig. 8), they would percolate downward until they reached an impermeable layer (*e.g.,* colder ice; Fig. 7), potentially producing a highly saline region within the ice.

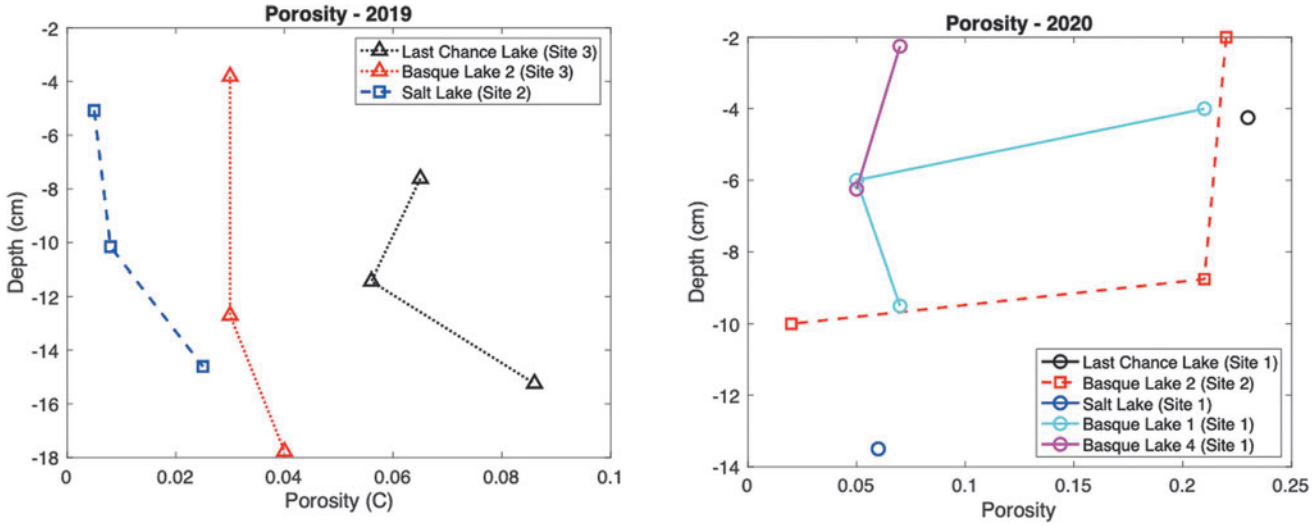

FIG. 11. Porosity profiles within the lake ice covers. (Left) Porosity of the lake ice covers during February 2019. (Right) Porosity of the lake ice covers during February 2020. Symbols and colors correspond to those presented in the temperature profile plots of Fig. 7.

This high salinity region could lead to the dissolution of the surrounding ice, ultimately producing the observed internal brine layer. It is interesting that many of the estimated porosities are near the sea ice percolation threshold (ϕ_c) of $\sim$0.05, predicted by Golden *et al.* (2007). This suggests that solutes are mobile in the ice cover when $\phi > \phi_c$, and when freezing occurs salination of the interstitial fluid leads to gravity drainage (Notz and Worster, 2009) and freshening of the pore fluid. This allows for continued freezing of the ice layer. However, once the porosity is $\sim$0.05 ($\phi \approx \phi_c$) the percolation limit is reached and fluid flow within the ice is drastically reduced, preventing freshening of the pore fluid via gravity drainage and inducing a slower continued freezing rate of the residual brine as it is further concentrated (*i.e.,* its freezing point is further reduced), resulting in the clustering of porosities around 0.05. Porosities $\sim$0.05 are in the range observed for seawater-derived ices at similar temperatures (Golden *et al.*, 2007).

This is expected even for the amplified ion concentrations in the $MgSO_4$-dominated ices, as $MgSO_4$ has less of an impact on freezing point depression than does NaCl. This chemistry-dependent variability in freezing point depression is also evidenced by the amplified porosities (and lower minimum brine temperatures) seen at Last Chance Lake, which has a higher concentration of NaCl. The implications of porosity for material transport, astrobiology, and the geophysics of planetary ices are discussed in Section 4.

4. Discussion

The compositionally diverse hypersaline lakes of south-central British Columbia offer a unique analog laboratory to constrain the physicochemical properties and dynamics of planetary relevant ice-brine systems. The identification of relationships between the bioburden and ionic composition of chemically diverse ices, their formation histories, and their underlying parent fluid properties as well as the observation of thermophysical features theorized to occur in planetary ice-brine environments (*e.g.*, intra-ice hydrologic features, supercooling, salt hydrate precipitation) have both geophysical and astrobiological implication for icy worlds in our solar system.

4.1. Physicochemical and biological stratigraphy of the ice-brine systems

The general trends in major ion content, cell density (bioburden), porosity, and permeability suggest a dynamic ice cover that is capable of fluid, solute, and biological transport. As the ice solidifies, rejects salts into interstitial brine veins and pockets, and the brine concentrates, the system becomes gravitationally unstable and the interstitial brine convects downward into the underlying brine reservoir, forming brine channels in the ice (Fig. 5) (Buffo *et al.*, 2021a). The freshened ice can thus continue freezing, leading to a trend of increasing porosity and permeability with depth in the ice cover. Although the upper layers of the ice cover typically possess lower bulk ion concentrations than the underlying fluid, the remaining salts are likely concentrated in residual brine pockets, making any liquid regions in the upper ice column highly saline and potentially less hospitable to any resident organisms.

The same cryoconcentrative process could affect the pH of the residual brine as well, meaning the more neutral (relative to the underlying brine) pH values measured in many of the bulk ice samples (Supplementary Table S1) may underrepresent the alkalinity of the brine pockets/channels. The lower liquid content, generally colder temperature, and potentially chaotropic and/or hyperalkaline brine in the upper layers of the ice suggest that lower portions of the ice cover are likely to provide greener pastures for any biology present in the system (a trend mirrored in fresh lake ice [Santibáñez *et al.*, 2019] and sea ice [Thomas and Dieckmann, 2003; Loose *et al.*, 2011; Tedesco and Vichi, 2014]).

Indeed, the bioburden profiles of all the lake ice covers show amplified cell densities in the basal ice and underlying brine. In the case of Salt Lake, the highest cell density in the ice-brine system was observed within the basal ice layer. This is consistent with observations of sea ice, where volumetric ice algae densities in the lower layer of the ice column typically far exceed those of the underlying ocean (Ackley and Sullivan, 1994; Spindler, 1994).

This feature may have been most prominent at Salt Lake due to the deeper (>20 cm) underlying water column, as the benefits of colonizing the porous basal ice layer may not have been as prevalent in the shallower lakes due to the proximity of the brine-sediment interface—another advantageous substrate for biology to thrive within. It is important to note that there was appreciable biology present in all samples, including the shallow ice regions.

Although exploration of the viability of cells located in different regions of the ice cover was beyond the scope of this study, our results suggest that substantial bioburden (viable or not) is entrained in diverse saline ices and that the density of the entrained bioburden is related to the ice formation history and underlying brine properties (*e.g.*, brine chemistry, brine bioburden, ice liquid fraction). A similar quantitative relationship between salt entrainment and ice formation history has been shown to be important in describing the geochemistry of planetary ice shells (Hammond *et al.*, 2018; Buffo *et al.*, 2020; Vance *et al.*, 2020; Chivers *et al.*, 2021).

Constraining the rates of impurity entrainment in saline ices has important implications for our understanding of ice-ocean worlds, where ice shell geophysics depend critically on material properties of the ice (Pappalardo and Barr, 2004; Durham *et al.*, 2005; Han and Showman, 2005; McCarthy *et al.*, 2011), biosignature expression is dependent on the entrainment and transport dynamics of the ice shell (Schmidt *et al.*, 2017; Schmidt, 2020), and constraining the habitability of the underlying ocean will lean heavily on the interpretation of spacecraft measurements of the ice shell (Howell and Pappalardo, 2020).

4.2. The internal brine layer

The internal brine layer observed at Basque Lake 2 sample Site 2 is of substantial interest, as it supports the idea that high porosity water-rich regions may persist in the upper layers of an ice column. Although similar environments have been repeatedly observed in meteoric ice (*e.g.,* firn aquifers, brine infiltration into the McMurdo Ice Shelf), the occurrence of discrete internal brine layers in ocean/brine-derived ices is much more limited.

Brine layers have been observed in cryopegs (Gilichinsky *et al.*, 2003, 2005; Shimanov *et al.*, 2020; Iwahana *et al.*, 2021), marine permafrost (Colangelo-Lillis *et al.*, 2016), and a limited number of Antarctic Dry Valley lake ice covers (Priscu *et al.*, 1998). In the case of Basque Lake 2, a solid ice layer overlaid a discrete brine pocket, which we were able to drain by syringing brine out (<1 L total volume). The brine layer thickness varied locally from 0.5 to 2 cm in thickness.

The brine layer was not present at drill sites <1 m away, thus the brine layer was highly localized and not substantially connected to the basal brine layer (as there was no inflow into the voided pocket). We do not know the exact physical processes that would facilitate the generation of such an internal brine layer, but we propose that the eutectic melting of a high salinity region due to surface warming or pressurization of the underlying brine pool as potential mechanisms.

If there existed a region of enhanced salinity within the ice cover, warming from the surface could raise the internal ice temperature above its eutectic melting point, creating a localized melt pocket/sheet that would grow in volume through the dissolution of ice until the concentration of the melt pocket was such that its freezing point matched the local temperature. Such high salinity regions could form due to localized interstitial hydrate precipitation during a period of rapid ice formation, or from the collection of downwelling melt created by warm surface temperatures when it reached an impermeable layer.

The low temperature of the internal brine (−5.24°C), its similarity to the basal brine temperature (−5.11°C, which is likely at its saturation point), and their separation by a colder ice layer (−5.35°C) would support the latter theory. Conversely, over pressurization of the underlying brine pool could drive upward brine transport into porous regions of the ice cover.

The relatively small sizes of the brine pools, along with the low permeability of the surrounding sediments and underlying salt hydrate basements (Fig. 1), could facilitate over pressurization in the basal brine and force brine upward into the ice cover, where it would preferentially infiltrate porous regions/layers of the ice (akin to sill intrusion in magmatic systems). If the conduit sourcing the brine layer refroze, it could isolate the intra-ice brine, forming the observed feature.

While occurring on a smaller scale in the lake ice cover, these exact processes have been theorized as mechanisms that could induce analogous cryovolcanic/cryohydrologic processes in the ice shells of ice-ocean world (*e.g.,* lens formation via eutectic melting [Schmidt *et al.*, 2011], sill and dike formation via the intrusion of underlying ocean fluid [Michaut and Manga, 2014; Craft *et al.*, 2016]). Such near surface liquid environments would provide accessible targets for upcoming missions, which are important for both planetary exploration and planetary protection. As such, understanding the generation, distribution, longevity, and potential habitability of such features is imperative to constraining the spatiotemporal habitability of ice-ocean worlds and will inform mission design and data synthesis.

Similarly, salt-rich aqueous environments on both ancient (Fastook *et al.*, 2012; Fastook and Head, 2015; Ojha *et al.*, 2020) and present-day (Ojha *et al.*, 2015; Orosei *et al.*, 2018; Lauro *et al.*, 2021) Mars would likely be characterized by ice-brine systems, some of which are exceptionally similar to the Canadian lakes we visited (Fox-Powell *et al.*, 2016; Pontefract *et al.*, 2017, 2019; Fox-Powell and Cockell, 2018). These unique analog systems can be leveraged to improve habitability classifications for martian regions, quantify putative martian hydrological processes, and aid in the search for remnant, relict, and contemporary habitable environments.

4.3. Supercooling and salt hydrate formation

Another interesting process observed at the lakes is supercooling, the depression of a liquid below its freezing point. Evidence for supercooling can be seen in the seasonal evolution of brine temperatures at Basque Lake 2 and Last Chance Lake (Fig. 8). The minimum brine temperatures occur early in the season, likely before any basal salt hydrate layer is present (*e.g.,* in September 2019 there were no basal hydrates present at Last Chance Lake—compare with Supplementary Fig. S2).

The lack of nucleation sites for precipitation to occur requires the brine to supersaturate and supercool until the energy barrier for initial salt hydrate nucleation is overcome (Toner *et al.*, 2014). Once this minimum temperature is reached and an initial basal salt layer is established, further precipitation occurs at the eutectic temperature and concentration of the sub-ice brine (no supercooling is needed to facilitate further nucleation, as nucleation sites now exist).

This leads to stable brine temperatures, evident in both lakes for the remainder of the season (Fig. 8). Only minimal deflections in brine temperature occur, even under extreme surface temperature variability (*e.g.,* multiple days of surface temperatures ≤ −15°C during mid-January and multiple days of surface temperatures above the brine eutectic temperatures in early February). A principal explanation for the exceptional stability of the sub-ice brine temperatures is the large latent heat of fusion associated with the precipitation of both ice and salt hydrates, which can have a latent heat of formation that exceeds that of the ice-water phase transition by orders of magnitude (Grevel *et al.*, 2012).

A substantial heat source and sink, the energy associated with the phase change of these materials will buffer any drastic and rapid changes in brine temperature. In addition, the precipitation of salt hydrates on saturation of the sub-ice brine substantially increases the longevity of the fluid reservoir, as all of the heat associated with the latent heat of formation of the hydrates must also be lost from the system before solidification of the brine can continue. This is supported by ice thickness measurements of Little Salt Pond, a substantially less saline spring-fed pool adjacent to Salt Lake (~100 m), which exhibited an ice thickness of 31 cm compared with Salt Lake's measured ice thicknesses of 18 and 18.5 cm.

Supercooling and salt hydrate precipitation have important implications for low-temperature saline systems on Earth, Mars, and ice-ocean worlds. The observation of supercooling in naturally occurring brines on Earth gives credence to the possibility for analogous supercooled environments on other bodies (Toner *et al.*, 2014) and is a unique extremophilic habitat. If these supercooled environments can persist for geologically significant time scales, they could broaden the temperature limits where liquid water is stable, and thus the thermal window of the limits of life.

We note that the time scale over which the brines observed in this study remain supercooled is on the order of days; however, the Canadian lake systems are minimally buffered from the local extreme surface temperatures. If a brine system on Mars or Europa was buried in the subsurface regolith or ice shell, it would likely be subject to more gradual thermal variations and could potentially remain in a supercooled state for much longer.

The antifreeze potential associated with salt hydrate precipitation could be even more impactful. In $MgSO_4$ systems, one of the first stable hydrate phases is meridianiite ($MgSO_4 \cdot 11H_2O$). With a latent heat of formation (aqueous $\rightarrow$ solid) of 1.44e^7 J/kg (Grevel *et al.*, 2012) ($\sim$43 times that of ice), its precipitation releases an immense amount of heat into saturated $MgSO_4$ systems (*i.e.,* the lakes observed in this study). This suggests that if ice-brine systems reach saturation and begin to precipitate out salt hydrate phases, their continued solidification could be drastically impeded, significantly extending their lifetimes.

These salt-rich niches could provide stable (or quasi-stable) aqueous environments for halophilic psychrophiles, water activity, and chaotropicity permitting. Potential regions where this phenomenon could (have) occur(ed) include surface and shallow subsurface saline lakes and sediments on Mars (Toner *et al.*, 2014; Rapin *et al.*, 2019), subglacial martian lakes (Orosei *et al.*, 2018; Sori and Bramson, 2019; Lauro *et al.*, 2021) similar to some terrestrial hypersaline subglacial systems (Rutishauser *et al.*, 2018), and hydrological brine features in the ice shells of ice-ocean worlds (*e.g.,* lenses and lenticulae [Schmidt *et al.*, 2011; Chivers *et al.*, 2021], sills, dikes, porous regions [Buffo *et al.*, 2020]).

Constraining the physical, biological, and chemical dynamics of these understudied analog environments will feed directly into forward models of planetary ice-brine environments aimed at quantifying their spatiotemporal evolution, habitability, and dynamic processes.

The presence of salt hydrates in ice-brine systems can add additional geochemical complexities. When salt hydrates precipitate out of solution, they introduce new phases to the system and alter the chemistry of the remaining brine. Much like fractional crystallization in magmatic systems, this can result in chemical heterogeneity of the resulting solid and will govern the chemical evolution of the residual melt (Fox-Powell and Cousins, 2021).

In analogy with terrestrial petrology of the mantle and lithosphere, minimal variations in melt fraction and composition can have substantial impacts on the thermal and mechanical properties of planetary ice shells (McKenzie, 1989; Buffo *et al.*, 2021b). Further, models aimed at interpreting the relationship between ice composition and parent fluid composition and/or habitability (*e.g.*, linking surface ice or plume particle composition to interior ocean composition) should address the potential effects of salt hydrate precipitation dynamics as fractional crystallization could alter the results (Buffo *et al.*, 2020; Fox-Powell *et al.*, 2020; Fox-Powell and Cousins, 2021).

Currently, dynamic models of planetary ices and ice-ocean world systems do not account for the presence or effects of salt hydrates (Buffo *et al.*, 2020, 2021b; Vance *et al.*, 2020). British Columbia's saline lakes provide a unique opportunity to investigate the salt hydrate dynamics within diverse natural ice-brine systems, including salt hydrate precipitation in a saturating reservoir and the presence and geochemical dynamics of salt hydrates in diverse ices. Such results can be leveraged as benchmarks for more accurate models hoping to include the geochemical and thermophysical dynamics of ternary ice-brine-hydrate systems.

5. Conclusion

The hypersaline lakes of British Columbia's Cariboo Plateau comprise an exceptional terrestrial analog for planetary ice-brine systems. The range of lake chemistries and concentrations, coupled with intense winters, produces a compositionally diverse spectrum of lake ice covers. The novel observations resulting from these field expeditions expand our understanding of the biogeochemistry of relatively understudied, but broadly applicable, terrestrial analog systems, as ice-brine environments are likely ubiquitous throughout the solar system (*e.g.*, Mars, Europa, Enceladus, etc.).

Moreover, this study provides a methodology for quantifying the habitability of planetary ices that can be utilized to inform upcoming astrobiology mission planning and data analysis.

Our investigations provide insights into the relationships between both the bioburden and ionic composition of chemically diverse ices, their formation history, and their underlying parent fluid properties. This is most evident in the depth-dependent trends of biological entrainment, ion entrainment, and permeability. Our results show that the characteristics of these salt-rich lake ices follow similar trends to those observed in sea ice, which suggests that material entrainment is (1) inversely proportional to thermal gradients at the ice-ocean/brine interface (equivalently ice thickness), (2) proportional to the concentration of the parent ocean/brine reservoir, and (3) depends critically on the dynamics occurring in the gradient-rich multiphase layer near the base of the ice cover (Nakawo and Sinha, 1981; Eicken, 1992; Golden *et al.*, 2007; Notz and Worster, 2008; Hunke *et al.*, 2011; Buffo *et al.*, 2018).

Effectively, this work suggests that the physical mechanisms that govern the fractionation of liquids, solids, and biota within diverse ices are similar yet dependent on composition. Such a result implies that the infusion of these dynamics into models of planetary ice processes and the analysis of planetary data sets is well founded, granted that the larger spatiotemporal scales of planetary ice-brine systems are accounted for (Buffo *et al.* (2020, 2021b)).

In addition, we observed a number of novel features in naturally occurring ice-brine environments that have important geophysical and astrobiological implications for both terrestrial and planetary cryohydrologic systems; these include internal brine layers in the ice cover of Basque Lake 2, widespread and heterogeneous salt hydrate precipitation and the associated effects of their latent heat of fusion on brine longevity and resistance to solidification, and the likely supercooling of brines in a natural setting.

Future work will utilize the collected profiles to validate reactive transport models of planetary ice formation and evolution (Brown *et al.*, 2020b; Buffo *et al.*, 2020) that seek to simulate the thermal and physicochemical properties of diverse ice-brine systems. Physicochemical heterogeneities

likely play an important role in ice shell geophysical processes (Pappalardo and Barr, 2004; Barr and McKinnon, 2007; Schmidt *et al.*, 2011; Johnson *et al.*, 2017), and proliferous biological communities are sustained by physical and thermochemical gradients in terrestrial ice-ocean/brine environments (Loose *et al.*, 2011; Daly *et al.*, 2013). As such, devising methods and models that quantify the thermophysical, biological, and geochemical properties and dynamics of planetary ices has implications for constraining the geophysics of icy worlds and assessing the spatiotemporal habitability of their ice-brine systems.

This study is of particular importance due to the presence of $MgSO_4$ and Na_2CO_3 in the ice. With potentially similar ice chemistries existing on a number of high-priority astrobiology targets (Mars, Europa, Enceladus), constraining the characteristics and evolution of these analog ice-brine systems has direct implications for relating spacecraft observations of surface and ice shell properties to interior ocean/brine properties, as this relies heavily on quantifying the efficiency with which impurities are entrained and transported within the ice shell.

With any potential ocean-derived biosignatures subject to similar transport processes, impurity entrainment estimates feed forward into detection limit requirements of any future ice-ocean world surface missions. The empirical data set presented here provides a unique benchmark to validate geophysical and biogeochemical models of planetary ices, a crucial tool in forecasting the dynamics, properties, and habitability of ice-ocean worlds.

With a number of upcoming ice-ocean world missions promising to return observations with orders of magnitude higher spatial and spectral resolution than their predecessors and more *in situ* techniques, leveraging terrestrial analog systems such as British Columbia's hypersaline lakes can provide useful guides for the interpretation of data by linking measurements of ice composition to its thermodynamic history, parent fluid properties, and habitability.

Authors' Contributions

J.J.B. aided in the collection and analysis of all samples and field measurements, carried out PHREEQC simulations, and led the writing and editing of the article. E.K.B. aided in the collection and analysis of all samples and field measurements and participated in writing and editing the article. A.P. provided logistical support for the field work in 2019, aided in the collection and analysis of all samples and field measurements, and participated in writing and editing the article. B.E.S. aided in the analysis of all samples and field measurements, assisted in planning field work methods, and participated in writing and editing the article. B.K. aided in the flow cytometry analysis of the field samples and participated in writing and editing the article. J.L. aided in the analysis of all samples and field measurements, assisted in planning field work methods, and participated in writing and editing the article. J.B. aided in the flow cytometry analysis of the field samples, assisted in planning field work methods, and participated in writing and editing the article. M.G. aided in the ionic composition analysis of samples, assisted in planning field work methods, and participated in editing the article. J.B.G. aided in the fluorescence microscopy analysis of samples, assisted in planning field work methods, and participated in editing the article. T.P. aided in the analysis of field samples. C.C. aided in the writing of the porosity and permeability sections of the article. P.D. aided in the collection of sample and field measurements.

Author Disclosure Statement

No competing financial interests exist.

Funding Information

Jacob J. Buffo, Emma K. Brown, Alexandra Pontefract, Britney E. Schmidt, Benjamin Klempay, Justin Lawrence, Jeff Bowman, Jennifer B. Glass, and Peter Doran were funded by the NASA Network for Life Detection project Oceans Across Space and Time (Grant No. 80NSSC18K1301). Jacob J. Buffo and Emma K. Brown were additionally funded through an American Philosophical Society Lewis and Clark Fund for Exploration and Field Research in Astrobiology grant (Title: *Biosignature Dynamics in British Columbia's Frozen Hypersaline Lakes: Implications for the Habitability and Bioburden of Ice-Brine Environments*). Alexandra Pontefract was also supported by NASA Exobiology grant, *Biosignature Preservation in Sulfate Dominated Environments* (Grant No. 80NSSC20K0849).

Supplementary Material

Supplementary Material
Supplementary Figure S1
Supplementary Figure S2
Supplementary Figure S3
Supplementary Table S1
Supplementary Table S2

References

Ackley SF and Sullivan CW (1994) Physical controls on the development and characteristics of Antarctic sea-ice biological communities—a review and synthesis. *Deep Sea Res Part I Oceanogr Res Pap* 41:1583–1604.

Barr AC and McKinnon WB (2007) Convection in ice I shells and mantles with self-consistent grain size. *J Geophys Res Planets* 112:02781.

Bauer JM, Buratti BJ, Li JY, *et al.* (2010) Direct detection of seasonal changes on triton with hubble space telescope. *Astrophys J Lett* 723:L49–L52.

Bear J (2013) *Dynamics of Fluids in Porous Media*. Courier Corporation, North Chelmsford, MA.

Brown E, Buffo J, Grantham M, *et al.* (2020a) Trapped in the ice: an analysis of brines in British Columbia's hypersaline lakes. In *LPI* (2326):2218.

Brown EK, Buffo J, Schmidt B, *et al.* (2020b) Trapped in the ice: an analysis of brines in British Columbia's hypersaline lakes. In *Lunar and Planetary Science Conference*. Woodlands, TX.

Buczkowski DL, Scully JE, Quick L, *et al.* (2019) Tectonic analysis of fracturing associated with Occator crater, *Icarus* 320:49–59.

Buffo JJ (2019) *Multiphase Reactive Transport in Planetary Ices*. Georgia Institute of Technology, Georgia.

Buffo JJ, Schmidt BE, and Huber C (2018) Multiphase reactive transport and platelet ice accretion in the sea ice of McMurdo sound, Antarctica. *J Geophys Res Oceans* 123:324–345.

Buffo J, Schmidt B, Pontefract A, *et al.* (2019) Frozen fingerprints: chemical and biological entrainment in planetary ices. In *Astrobiology Science Conference*. Bellevue, Washington.

Buffo J, Schmidt B, Huber C, and Walker CC (2020) Entrainment and dynamics of ocean-derived impurities within Europa's ice shell. *JGR Planets* 125.

Buffo J, Schmidt B, Huber C, *et al.* (2021a) Characterizing the ice-ocean interface of icy worlds: a theoretical approach. *Icarus* 360:114318.

Buffo JJ, Meyer CR, Parkinson JR, *et al.* (2021b) Dynamics of a solidifying icy satellite shell. *JGR Planets* 126.

Čadek O, Tobie G, Van Hoolst T, *et al.* (2016) Enceladus's internal ocean and ice shell constrained from Cassini gravity, shape, and libration data. *Geophys Res Lett* 43:5653–5660.

Carr MH (1987) Water on Mars. *Nature* 32630–32635.

Castillo-Rogez J (2020) Future exploration of Ceres as an ocean world. *Nat Astron* 4:732–734.

Castillo-Rogez JC, Hesse M, Formisano M, *et al.* (2019) Conditions for the long-term preservation of a deep brine reservoir in Ceres. *Geophys Res Lett* 46:1963–1972.

Castillo-Rogez JC, Neveu M, Scully JE, *et al.* (2020) Ceres: astrobiological target and possible ocean world. *Astrobiology* 20:269–291.

Chivers C, Buffo J, and Schmidt B (2021) Thermal and chemical evolution of small, shallow water bodies on europa. *JGR Planets* 2326:1047.

Colangelo-Lillis J, Eicken H, Carpenter S, *et al.* (2016) Evidence for marine origin and microbial-viral habitability of sub-zero hypersaline aqueous inclusions within permafrost near Barrow, Alaska. *FEMS Microbiol Ecol* 92: fiw053.

Cosciotti B, Balbi A, Ceccarelli A, *et al.* (2019) Survivability of anhydrobiotic Cyanobacteria in salty ice: implications for the habitability of icy worlds. *Life (Basel)* 9:86.

Cottier F, Eicken H, and Wadhams P (1999) Linkages between salinity and brine channel distribution in young sea ice. *J Geophys Res Oceans* 104:15859–15871.

Cox GF and Weeks WF (1974) Salinity variations in sea ice. *J Glaciol* 13:109–120.

Craft KL, Patterson GW, Lowell RP, *et al.* (2016) Fracturing and flow: investigations on the formation of shallow water sills on Europa. *Icarus* 274:297–313.

Daly M, Rack F, and Zook R (2013) *Edwardsiella andrillae*, a new species of sea anemone from Antarctic ice. *PLoS One* 8: e83476.

Di Paolo F, Lauro SE, Castelletti D, *et al.* (2016) Radar signal penetration and horizons detection on Europa through numerical simulations. *IEEE J Sel Top Appl Earth Obs Remote Sens* 10:118–129.

Doran PT, Fritsen CH, McKay CP, *et al.* (2003) Formation and character of an ancient 19-m ice cover and underlying trapped brine in an ''ice-sealed'' east Antarctic lake. *Proc Natl Acad Sci U S A* 100:26–31.

Durham WB, Stern LA, Kubo T, *et al.* (2005) Flow strength of highly hydrated Mg-and Na-sulfate hydrate salts, pure and in mixtures with water ice, with application to Europa. *J Geophys Res Planets* 110.

Eicken H (1992) Salinity profiles of Antarctic sea ice—field data and model results. *J Geophys Res Oceans* 97:15545–15557.

Ellis B, Haaland P, Hahne F, *et al.* (2009) flowCore: basic structures for flow cytometry data. *R Package Version* 1.

Fanale FP, Granahan JC, McCord TB, *et al.* (1999) Galileo's multiinstrument spectral view of Europa's surface composition. *Icarus* 139:179–188.

Fastook JL and Head JW (2015) Glaciation in the Late Noachian Icy Highlands: ice accumulation, distribution, flow rates, basal melting, and top-down melting rates and patterns. *Planet Space Sci* 106:82–98.

Fastook JL, Head JW, Marchant DR, *et al.* (2012) Early Mars climate near the Noachian–Hesperian boundary: independent evidence for cold conditions from basal melting of the south polar ice sheet (Dorsa Argentea Formation) and implications for valley network formation. *Icarus* 219:25–40.

Feltham DL, Untersteiner N, Wettlaufer JS, and Worster MG (2006) Sea ice is a mushy layer. *Geophys Res Lett* 33, L14501, doi:10.1029/2006GL026290

Fisher LA, Pontefract A, Som S, *et al.* (2021) Current state of athalassohaline deep sea hypersaline anoxic basin (DHAB) research–recommendations for future work and relevance to astrobiology. *Environ Microbiol* 23(7):3360–3369.

Foster IS, King PL, Hyde BC, *et al.* (2010) Characterization of halophiles in natural MgSO4 salts and laboratory enrichment samples: astrobiological implications for Mars. *Planet Space Sci* 58:599–615.

Fox-Powell MG and Cockell CS (2018) Building a geochemical view of microbial salt tolerance: halophilic adaptation of *Marinococcus* in a natural magnesium sulfate brine. *Front Microbiol* 9:739.

Fox-Powell MG and Cousins C (2021) Partitioning of crystalline and amorphous phases during freezing of simulated Enceladus ocean fluids. *J Geophys Res Planets* 126:e2020JE006628.

Fox-Powell MG, Hallsworth JE, Cousins CR, *et al.* (2016) Ionic strength is a barrier to the habitability of mars. *Astrobiology* 16:427–442.

Fox-Powell MG, Hamp R, Schwenzer SP, *et al.* (2020) Phase fractionation and the fate of bioessential elements during freezing of simulated Enceladus ocean fluids. In *AGU Fall Meeting*.

Freitag J and Eicken H (2003) Meltwater circulation and permeability of Arctic summer sea ice derived from hydrological field experiments. *J Glaciol* 49:349–358.

Gilichinsky D, Rivkina E, Bakermans C, *et al.* (2005) Biodiversity of cryopegs in permafrost. *FEMS Microbiol Ecol* 53:117–128.

Gilichinsky D, Rivkina E, Shcherbakova V, *et al.* (2003) Supercooled water brines within permafrost—an unknown ecological niche for microorganisms: a model for astrobiology. *Astrobiology* 3:331–341.

Glein CR, Baross JA, and Waite JH (2015) The pH of Enceladus' ocean. *Geochim Cosmochim Acta* 162:202–219.

Golden KM, Ackley SF, and Lytle VV (1998) The percolation phase transition in sea Ice. *Science* 282:2238–2241.

Golden KM, Eicken H, Heaton AL, *et al.* (2007) Thermal evolution of permeability and microstructure in sea ice. *Geophys Res Lett* 34:gl030447.

Grau Galofre A, Jellinek AM, and Osinski GR (2020) Valley formation on early Mars by subglacial and fluvial erosion. *Nat Geosci* 13:663–668.

Grevel K-D, Majzlan J, Benisek A, *et al.* (2012) Experimentally determined standard thermodynamic properties of synthetic MgSO4 · 4H2O (starkeyite) and MgSO4 · 3H2O: a revised internally consistent thermodynamic data set for magnesium sulfate hydrates. *Astrobiology* 12:1042–1054.

Hallsworth JE, Yakimov MM, Golyshin PN, *et al.* (2007) Limits of life in MgCl2-containing environments: chaotropicity defines the window. *Environ Microbiol* 9:801–813.

Hammond NP, Parmenteir E, and Barr AC (2018) Compaction and melt transport in ammonia-rich ice shells: implications for the evolution of triton. *J Geophys Res Planets* 123:3105–3118.

Han L and Showman AP (2005) Thermo-compositional convection in Europa's icy shell with salinity. *Geophys Res Lett* 32: L20201. doi: 10.1029/2005GL023979.

Howell SM and Pappalardo RT (2018) Band formation and ocean-surface interaction on Europa and Ganymede. *Geophys Res Lett* 45:4701:4709.

Howell SM and Pappalardo RT (2020) NASA's Europa Clipper-a mission to a potentially habitable ocean world. *Nat Commun* 11:1311.

Hunke EC, Notz D, Turner AK, *et al.* (2011) The multiphase physics of sea ice: a review for model developers. *Cryosphere* 5:989–1009.

Iwahana G, Cooper ZS, Carpenter SD, *et al.* (2021) Intra-ice and intra-sediment cryopeg brine occurrence in permafrost near Utqiaġvik (Barrow). *Permafrost Periglacial Process* 32: 427–446.

Jenkins OP (1918) Spotted lakes of epsomite in Washington and British Columbia. *Am J Sci* 46:638–644.

Johnson BC, Sheppard RY, Pascuzzo AC, *et al.* (2017) Porosity and salt content determine if subduction can occur in Europa's ice shell. *J Geophys Res Planets* 122:2765–2778.

Journaux B, Brown JM, Pakhomova A, *et al.* (2020) Holistic approach for studying planetary hydrospheres: Gibbs representation of ices thermodynamics, elasticity, and the water phase diagram to 2,300 MPa. *J Geophys Res Planets* 125: e2019JE006176.

Kalousova K, Schroeder DM, and Soderlund KM (2017) Radar attenuation in Europa's ice shell: obstacles and opportunities for constraining the shell thickness and its thermal structure. *J Geophys Res Planets* 122:524–545.

Kargel JS, Kaye JZ, Head JW, *et al.* (2000) Europa's crust and ocean: origin, composition, and the prospects for life. *Icarus* 148:226–265.

Klempay B, Arandia-Gorostidi N, Dekas AE, *et al.* (2021) Microbial diversity and activity in Southern California salterns and bitterns: analogues for remnant ocean worlds. *Environ Microbiol* 23(7):3825-3839.

Lauro SE, Pettinelli E, Caprarelli G, *et al.* (2021) Multiple subglacial water bodies below the south pole of Mars unveiled by new MARSIS data. *Nat Astron* 5:63–70.

Loose B, Miller LA, Elliott S, *et al.* (2011) Sea ice biogeochemistry and material transport across the frozen interface. *Oceanography* 24:202–218.

Malmgren F (1927) *On the Properties of Sea-Ice.* Bergen, A/S John Griegs Boktrykkeri.

Marion G, Farren R, and Komrowski A (1999) Alternative pathways for seawater freezing. *Cold Regions Sci Technol* 29: 259–266.

Marion GM, Fritsen CH, Eicken H, *et al.* (2003) The search for life on Europa: limiting environmental factors, potential habitats, and Earth analogues. *Astrobiology* 3:785–811.

Maus S, Schneebeli M, and Wiegmann A (2020) An X-ray micro-tomographic study of the pore space, permeability and percolation threshold of young sea ice. *The Cryosphere* 15: 4047–4072.

McCarthy C, Cooper RF, Goldsby DL, *et al.* (2011) Transient and steady state creep response of ice I and magnesium sulfate hydrate eutectic aggregates. *J Geophys Res Planets* 116: 003689.

McKenzie D (1989) Some remarks on the movement of small melt fractions in the mantle. *Earth Planet Sci Lett* 95:53–72.

McKinnon WB (1999) Convective instability in Europa's floating ice shell. *Geophys Res Lett* 26:951–954.

Michaut C and Manga M (2014) Domes, pits, and small chaos on Europa produced by water sills. *J Geophys Res Planets* 119:550–573.

Murray AE, Kenig F, Fristen CH, *et al.* (2012) Microbial life at -13 degrees C in the brine of an ice-sealed Antarctic lake. *Proc Natl Acad Sci U S A* 109:20626–20631.

Nakawo M and Sinha NK (1981) Growth rate and salinity profile of first-year sea ice in the high Arctic. *J Glaciol* 27: 315–330.

Nathan E, Berton M, Girona T, *et al.* (2019) The freezing and fracture of icy satellites: experimental analog and stress analysis. *AGUFM* 2019:P53D-3489.

Nimmo F and Pappalardo RT (2006) Diapir-induced reorientation of Saturn's moon Enceladus. *Nature* 441:614–616.

Nimmo F and Schenk P (2006) Normal faulting on Europa: implications for ice shell properties. *J Struct Geol* 28:2194–2203.

Notz D and Worster MG (2008) In situ measurements of the evolution of young sea ice. *J Geophys Res Oceans* 113: jc004333.

Notz D and Worster MG (2009) Desalination processes of sea ice revisited, *J Geophys Res Oceans* 114:jc004885.

Ojha L, Buffo J, Karunatillake S, and Siegler M (2020) Groundwater production from geothermal heating on early mars and implications for early Matian habitability. *Sci Adv* 6:eabb1669.

Ojha L, Wilhelm MB, Murchie SL, *et al.* (2015) Spectral evidence for hydrated salts in recurring slope lineae on Mars. *Nat Geosci* 8:829.

Oren A (2013) Life in magnesium-and calcium-rich hypersaline environments: salt stress by chaotropic ions. In *Polyextremophiles* (edited by ML Capese, E Clark, IK Salah, *et al.*) Springer, Dordrecht, pp 215–232.

Orosei R, Lauro SE, Pettinelli E, *et al.* (2018) Radar evidence of subglacial liquid water on Mars. *Science* 361:490–493.

Pappalardo RT and Barr AC (2004) The origin of domes on Europa: the role of thermally induced compositional diapirism. *Geophys Res Lett* 31:19202.

Parkhurst DL and Appelo C (1999) User's guide to PHREEQC (Version 2): a computer program for speciation, batch-reaction, one-dimensional transport, and inverse geochemical calculations. *Water Resour Investig Rep* 99:312.

Parkhurst DL and Appelo C (2013) *Description of Input and Examples for PHREEQC Version 3: A Computer Program for Speciation, Batch-Reaction, One-Dimensional Transport, and Inverse Geochemical Calculations*. Rep. 2328-7055, US Geological Survey.

Parkinson CD, Liang MC, Yung YL, *et al.* (2008) Habitability of enceladus: planetary conditions for life. *Orig Life Evol Biosph* 38:355–369.

Peterson RA and Krantz WB (2008) Differential frost heave model for patterned ground formation: corroboration with observations along a North American arctic transect. *J Geophys Res Biogeosci* 113:00059.

Pontefract A, Carr CE, and Osburn MR (2019) The role of ionic composition and concentration on biosignature preservation: lessons from the ''Spotted'' Lakes of British Colombia. In *Paper Presented at 2019 Astrobiology Science Conference, AGU.*

Pontefract A, Zhu TF, Walker VK, *et al.* (2017) Microbial diversity in a hypersaline sulfate lake: a terrestrial analog of ancient Mars. *Front Microbiol* 8:1819.

Priscu JC, Fritsen CH, Adams EE, *et al.* (1998) Perennial Antarctic lake ice: an oasis for life in a polar desert. *Science* 280:2095–2098.
Priscu JC and Hand KP (2012) Microbial habitability of icy worlds. *Microbe* 7:167–172.
Quick LC, Buczkowski DL, Ruesch O, *et al.* (2019) A possible brine reservoir beneath Occator Crater: thermal and compositional evolution and formation of the Cerealia Dome and Vinalia Faculae. *Icarus* 320:119–135.
Rapin W, Ehlmann BL, Dromart G, *et al.* (2019) An interval of high salinity in ancient Gale crater lake on Mars. *Nat Geosci* 12:889.
Renaut RW and Long PR (1989) Sedimentology of the saline lakes of the Cariboo Plateau, interior British-Columbia, Canada. *Sediment Geol* 64:239–264.
Rutishauser A, Blankenship DD, Sharp M, *et al.* (2018) Discovery of a hypersaline subglacial lake complex beneath Devon Ice Cap, Canadian Arctic. *Sci Adv* 4:eaar4353.
Santibáñez PA, Michaud AB, Vick-Majors TJ, *et al.* (2019) Differential incorporation of bacteria, organic matter, and inorganic ions into lake ice during ice formation. *J Geophys Res Biogeosci* 124:385–600.
Schenk P, Sizemore HG, Schmidt B, *et al.* (2019) The central pit and dome at Cerealia Facula bright deposit and floor deposits in Occator crater, Ceres: morphology, comparisons and formation. *Icarus* 320:159–187.
Schmidt BE (2020) The astrobiology of Europa and the Jovian System. In: *Planet Astrobiology* (edited by V Meadows *et al.*) pp 185–215.
Schmidt BE, Blankenship DD, Patterson GW, and Schenk PM (2011) Active formation of 'chaos terrain' over shallow subsurface water on Europa, *Nature* 479:502–505.
Schmidt BE, Buffo J, and Main Campus A (2017) Biomarker production and preservation on Europa. In *Paper Presented at European Planetary Science Congress*. EPSC2017-397
Scully CJE, Buczkowski DL, Raymond CA, *et al.* (2019) Ceres' Occator crater and its faculae explored through geologic mapping. *Icarus* 320:7–23.
Shimanov A, Komarov I, and Kireeva T (2020) Peculiarities of the changes in chemical composition of cryopegs of the Yamal Peninsula during cryogenic concentration. *Moscow Univ Geol Bull* 75:72–79.
Sori MM and Bramson AM (2019) Water on Mars, with a grain of salt: local heat anomalies are required for basal melting of ice at the South pole today. *Geophys Res Lett* 46:1222–1231.
Sotin C and Tobie G (2004) Internal structure and dynamics of the large icy satellites. *Comptes Rendus Phys* 5:769–780.
Sparks WB, Hand KP, McGrath MA, *et al.* (2016) Probing for evidence of plumes on Europa with Hst/Stis. *Astrophys J* 829: 121.
Spindler M (1994) Notes on the biology of sea-ice in the Arctic and Antarctic. *Polar Biol* 14:319–324.
Srivastava A, Pearson VK, Schwenzer SP, *et al.* (2021) Are sulfates the viable substrates for the long-term preservation of lipids on Mars?, In *52nd Lunar and Planetary Science Conference 2021* (LPI Contrib. No. 2548)
Stevens AH and Cockell CS (2020) A systematic study of the limits of life in mixed ion solutions: physicochemical parameters do not predict habitability. *Frontiers in Microbiology* 11:1478.
Tedesco L and Vichi M (2014) Sea ice biogeochemistry: a guide for modelers. *PLoS One* 9:e89217.
Thomas DN and Dieckmann GS (2003) Biogeochemistry of Antarctic sea ice. In *Oceanography and Marine Biology, An Annual Review, vol 40* edited by RN Gibson, M Barnes, and RIA Atkinson. CRC Press, London, pp 151–156.
Toner JD, Catling DC, and Light B (2014) The formation of supercooled brines, viscous liquids, and low-temperature perchlorate glasses in aqueous solutions relevant to Mars. *Icarus* 233:36–47.
Tosca NJ, Knoll AH, and McLennan SM (2008) Water activity and the challenge for life on early Mars. *Science* 320:1204–1207.
Vance SD, Journaux B, Hesse M, *et al.* (2020) The salty secrets of icy ocean worlds. *J Geophys Res Planets* 126: e2020JE006736.
Vaniman DT, Bish DL, Chipera SJ, *et al.* (2004) Magnesium sulphate salts and the history of water on Mars. *Nature* 431: 663–665.
Walker C, Schmidt B, and Bassis J (2014) Breaking the ice: on the application of fracture system mechanics and fragmentation theory to the chaos regions of Europa, *LPI* 1777: 2659.
Weeks WF and Ackley SF (1986) The growth, structure, and properties of sea ice. In *The Geophysics of Sea Ice* edited by N Untersteine. Springer, Boston, MA, pp 9–164.
Weller MB, Fuchs L, Becker TW, *et al.* (2019) Convection in thin shells of icy satellites: effects of latitudinal surface temperature variations. *J Geophys Res Planets* 124:2029–2053.
Wray J, Milliken R, Dundas CM, *et al.* (2011) Columbus crater and other possible groundwater-fed paleolakes of Terra Sirenum, Mars. *J Geophys Res Planets* 116. doi:10.1029/2010JE003694
Zolotov MY (2007) An oceanic composition on early and today's Enceladus. *Geophys Res Lett* 34:gl031234.
Zolotov MY and Shock EL (2001) Composition and stability of salts on the surface of Europa and their oceanic origin. *J Geophys Res Planets* 106:32815–32827.
Zorzano MP, Mateo-Marti E. Prieto-Ballesteros O, *et al.* (2009) Stability of liquid saline water on present day Mars. *Geophys Res Lett* 36:gl040315.

Address correspondence to:
Jacob J. Buffo
Thayer School of Engineering
Dartmouth College
14 Engineering Drive
Hanover, NH 03755-3529
USA

E-mail: jacobbuffo91@gmail.com

Submitted 3 June 2021
Accepted 12 March 2022
Associate Editor: John Rummel

Abbreviations Used

DAPI = 4′,6-diamidino-2-phenylindole
IC = ion chromatography
ICP-MS = ion coupled plasma mass spectrometry
$MgSO_4$ = magnesium sulfate
Na_2CO_3 = sodium carbonate
Na_2SO_4 = sodium sulfate
NaCl = sodium chloride
UV = ultraviolet